A Maxwellian Approach to Quantum Mechanics Explains the Nature of Free Electrons in Superfluid Helium

Randell L. Mills
BlackLight Power, Inc.
493 Old Trenton Road
Cranbury, NJ 08512

From the time of its inception, the quantum mechanical meaning of the electron wave function has been enigmatic, debated, and fluid. A now popular interpretation is a zero or one-dimensional point in an all-space probability wave function $\Psi(x)$ that only becomes "real" by act of measurement. However, the behavior of free electrons in superfluid helium has again forced the issue of the meaning of the wavefunction and its connection with reality. Electrons form bubbles in superfluid helium which reveal that the electron is real and that a physical interpretation of the wavefunction is necessary. It is time for the physical rather than the mathematical nature of the wavefunction to be determined. Using Maxwell's equations, the classical wave equation is solved with the constraint that a bound electron cannot radiate energy to give closed form physical solutions for the electron in atoms, the free electron, and the free electron in superfluid helium. The prediction of fractional principal quantum energy states of the electron in liquid helium and their behavior match the formerly inexplicable photoconductivity and mobility observations.

Phone: 609-490-1090; Fax: 609-490-1066; E-mail: rmills@blacklightpower.com

INTRODUCTION

Despite it successes, quantum mechanics (QM) has remained mysterious to all who have encountered it. Starting with Bohr and progressing into the present, the departure from intuitive, physical reality has widened. The connection between quantum mechanics and reality is more than just a "philosophical" issue. It reveals that quantum mechanics is not a correct or complete theory of the physical world and that inescapable internal inconsistencies and incongruities with physical observation arise when attempts are made to treat it as a physical as opposed to a purely mathematical "tool". Some of these issues are discussed in a review by Laloë [1].

Recently, the behavior of free electrons in superfluid helium has again forced the issue of the meaning of the wavefunction. Electrons form bubbles in superfluid helium which reveal that the electron is real and that a physical interpretation of the wavefunction is necessary. Furthermore, when irradiated with light of energy of about a 0.5 to several electron volts, the electrons carry current at different rates as if they exist with different sizes. It has been proposed that the behavior of free electrons in superfluid helium can be explained in terms of the electron breaking into pieces at superfluid helium temperatures [2]. Yet, the electron has proven to be indivisible even under particle accelerator collisions at 90 GeV (LEPII). The nature of the wavefunction must now be addressed. It is time for the physical rather than the mathematical nature of the wavefunction to be determined.

In an attempt to provide some physical insight into atomic problems and starting with the same essential physics as Bohr of e^- moving in the Coulombic field of the proton and the wave equation as modified by Schrodinger, a classical approach is explored which yields a model which is remarkably accurate and provides insight into physics on the atomic level. The proverbial view deeply seated in the wave-particle duality notion that there is no large-scale physical counterpart to the nature of the electron may not be correct. Physical laws and intuition may be restored when dealing with the wave equation and quantum mechanical problems. Specifically, using Maxwell's equations, the classical wave equation is solved with the constraint that a bound electron cannot radiate energy to give closed form physical solutions for the electron in atoms, the free electron, and the free electron in superfluid helium. The prediction of fractional principal quantum energy states of the electron in liquid helium match the photoconductivity and mobility observations without requiring that the electron is divisible.

DIVISIBLE ELECTRON?--IS QUANTUM MECHANICS ANY MORE THAN MATHEMATICAL?

In the 105 years since its discovery, there has been no evidence whatsoever that the electron is divisible. But, in order to explain, the rise in current of free electrons in superfluid helium when irradiated with low energy light and the observation of an unexpected plethora of exotic negative charge carriers in superfluid helium with mobilities greater than that of the normal electron, Maris [2] has proposed that the electron breaks into fractional pieces. Maris shows that the Schrödinger equation solution of the wavefunction of the $1p$ state, an excited state, will break into two following the $1s$ to $1p$ transition of an electron in superfluid helium. This result is a consequence of the localization of the maximum electron probability density, $\Psi(x)$, in the extremes of the dumb-bell shaped $1p$ orbital with the existence of a node at the center of the orbital. Maris likens $\Psi(x)$ to a physical electron density bubble. The large differences in time scales of the motion of the electron and the motion of the bubble wall means that the Franck-Condon principle should apply and that the wave function of the electron will deform adiabatically (Born-Oppenheimer principle) at this node to result in electron fission. Following the break, one half of the electron's wave function is trapped in each of the two daughter bubbles. As the wave function is the essence of an electron, the electron splits into two. One piece acquires all of the charge and the other is neutral.

Of course the electron can not break into two, and $\Psi(x)$ can not be an electron density function based on scattering experiments as point out by Max Born who formulated the currently accepted probability wave interpretation of $\Psi(x)$. However, experiments discussed in this paper reveal that electrons may be trapped in superfluid helium as autonomous electron bubbles interloped between helium atoms that have been excluded from the space occupied by the bubble. The surrounding helium atoms maintain the spherical bubble through van der Waals forces. Superfluid helium is an ideal medium to study individual trapped electrons in much the same way that individual ions may be studied in Penning traps. Both represent an ideal system to test quantum mechanics. Maris and other experimental physicists believe that the data on electrons in liquid helium reveals a fundamental flaw in quantum theory which has caused a furor [3-5]. Electrons bubbles in superfluid helium reveal that the electron is real and that a physical interpretation of the wavefunction is necessary. Physicists have always been content to think of the wave function, the unmeasurable entity which describes quantum systems, as a mathematical device with observable consequences. The time has come for the idea to be grounded in reality. For the electron bubbles in helium, Maris's position is that the size of the bubble is determined by how much of the wave function is trapped inside the bubble. If there is no part of the wave function inside the bubble, the bubble will collapse. This makes the wave function seem to be a tangible object. Theoreticians are going to have to address the question: what is a wave function? Is it a real thing, or just a mathematical convenience?" [5].

THE SCHRÖDINGER EQUATION REVISITED

The hydrogen atom is the only real problem for which the Schrödinger equation can be solved without approximations; however, it only provides three quantum numbers - not four, and inescapable disagreements between observation and predictions arise from the later postulated Dirac equation as well as the Schrödinger equation [6-8]. Furthermore, unlike physical laws such as Maxwell's equations, it is always disconcerting to those that study quantum mechanics that both must be accepted without any underlying physical basis for fundamental observables such as the stability of the hydrogen atom in the first place. In this instance, a circular argument regarding definitions for parameters in the wave equation solutions and the Rydberg series of spectral lines replaces a first-principles-based prediction of those lines [6-8]. Nevertheless, the application of the Schrödinger equation to real problems has provided useful approximations for physicists and chemists. Schrödinger interpreted $e\Psi^*(x)\Psi(x)$ as the charge-density or the amount of charge between x and $x+dx$ (Ψ^* is the complex conjugate of Ψ). Presumably, then, he pictured the electron to be spread over large regions of space. Three years after Schrödinger's interpretation, Max Born, who was working with scattering theory, found that this interpretation led to inconsistencies and he replaced the Schrödinger interpretation with the probability of finding the electron between x and $x+dx$ as

$$\int \Psi(x)\Psi^*(x)dx \tag{1}$$

Born's interpretation is generally accepted. Nonetheless, interpretation of the wave function is a never-ending source of confusion and conflict. Many scientists have solved this problem by conveniently adopting the Schrödinger interpretation for some problems and the Born interpretation for others. This duality allows the electron to be everywhere at one time—yet have no volume. Alternatively, the electron can be viewed as a discrete particle that moves here and there (from $r = 0$ to $r = \infty$), and $\Psi\Psi^*$ gives the time average of this motion. Despite its successes, after decades of futility, QM and the intrinsic Heisenberg Uncertainty Principle have not yielded a unified theory, are still purely mathematical, and have yet to be shown to be based in reality [8]. Both are based on circular arguments that the electron is a point with no volume with a vague probability wave requiring that the electron have multiple positions and energies including negative and infinite energies simultaneously. It may be time to revisit the 75 year old notion that fundamental particles such as the electron are one or zero dimensional and obey different physical laws than objects comprised of fundamental particles and the even more disturbing view that fundamental particles don't obey physical laws—rather they obey mathematics devoid of physical laws. Perhaps mathematics does not determine physics. It only models physics.

The Schrödinger equation was originally postulated in 1926 as having a solution of the one electron atom. It gives the principal energy levels of the hydrogen atom as eigenvalues of eigenfunction solutions of the Laguerre differential equation. But, as the principal quantum number n>>1, the eigenfunctions become nonsensical. Despite its wide acceptance, on deeper inspection, the Schrödinger equation solution is plagued with many failings as well as difficulties in terms of a physical interpretation that have caused it to remain controversial since its inception. Only the one electron atom may be solved without approximations, but it fails to predict electron spin and leads to models with nonsensical consequences such as negative energy states of the vacuum, infinities, and negative kinetic energy. In addition to many predictions, which simply do not agree with observations, the Schrödinger equation and succeeding extensions predict noncausality, nonlocality, spooky actions at a distance or quantum telepathy, perpetual motion, and many internal inconsistencies where contradicting statements have to be taken true simultaneously [6-8]. The behavior of free electrons in superfluid helium has again forced the issue of the meaning of the wavefunction, and a physical rather than a mathematical nature of the wavefunction is required since the observation is on the electron's physical form [2].

From the time of its inception, quantum mechanics (QM) has been controversial because its foundations are in conflict with physical laws and are internally inconsistent. Interpretations of quantum mechanics such as hidden variables, multiple worlds, consistency rules, and spontaneous collapse have been put forward in an attempt to base the theory in reality. Unfortunately many theoreticians ignore the requirement that the wave function must be real and physical in order for it to be considered a valid description of reality. For example, regarding this issue Fuchs and Peres believe [9] "Contrary to those desires, quantum theory does *not* describe physical reality. What it does is provide an algorithm for computing *probabilities* for macroscopic events ("detector ticks") that are the consequences of our experimental interventions. This strict definition of the scope of quantum theory is the only interpretation ever needed, whether by experimenters or theorists".

With Penning traps, it is possible to measure transitions including those with hyperfine levels of electrons of single ions. This case can be experimentally distinguished from statistics over equivalent transitions in many ions. Whether many or one, the transition energies are always identical within the resonant line width. So, *probabilities* have no place in describing atomic energy levels. Moreover, quantum theory is incompatible with probability theory since it is based on underlying unknown, but determined outcomes as discussed previously [8].

The Copenhagen interpretation provides another meaning of quantum mechanics. It asserts that what we observe is all we can know; any speculation about what an electron, photon, atom, or other atomic-sized entity is really is or what it is doing when we are not

looking is just that--speculation. The postulate of quantum measurement asserts that the process of measuring an observable forces it into a state of reality. In other words, reality is irrelevant until a measurement is made. In the case of electrons in helium, the fallacy with this position is that the "ticks" (migration times of electron bubbles) reveal that the electron is real before a measurement is made. Furthermore, experiments on transitions on single ions such as Ba^{+} in a Penning trap under continuous observation demonstrate that the postulate of quantum measurement of quantum mechanics is experimentally disproved as discussed previously [8, 10]. These issues and other such flawed philosophies and interpretations of experiments that arise from quantum mechanics were discussed previously [6-8].

QM gives correlations with experimental data. It does not explain the mechanism for the observed data. But, it should not be surprising that it gives good correlations given that the constraints of internal consistency and conformance to physical laws are removed for a wave equation with an infinite number of solutions wherein the solutions may be formulated as an infinite series of eigenfunctions with variable parameters. There are no physical constraints on the parameters. They may even correspond to unobservables such as virtual particles, hyperdimensions, effective nuclear charge, polarization of the vacuum, worm holes, spooky action at a distance, infinities, parallel universes, faster than light travel, etc. If you invoke the constraints of internal consistency and conformance to physical laws, quantum mechanics has never successfully solved a physical problem.

Throughout the history of quantum theory; wherever there was an advance to a new application, it was necessary to repeat a trial-and -error experimentation to find which method of calculation gave the right answers. Often the textbooks present only the successful procedure as if it followed from first principles; and do not mention the actual method by which it was found. In electromagnetic theory based on Maxwell's equations, one deduces the computational algorithm from the general principles. In quantum theory, the logic is just the opposite. One chooses the principle to fit the empirically successful algorithm. For example, we know that it required a great deal of art and tact over decades of effort to get correct predictions out of Quantum Electrodynamics (QED). For the right experimental numbers to emerge, one must do the calculation (i.e. subtract off the infinities) in one particular way and not in some other way that appears in principle equally valid. There is a corollary, noted by Kallen: from an inconsistent theory, any result may be derived.

Reanalysis of old experiments and many new experiments including electrons in superfluid helium challenge the Schrödinger equation predictions. Many noted physicists rejected quantum mechanics. Feynman also attempted to use first principles including Maxwell's Equations to discover new physics to replace quantum mechanics [11]. Other great physicists of the 20th century searched. "Einstein [...] insisted [...] that a more detailed,

wholly deterministic theory must underlie the vagaries of quantum mechanics" [12]. He felt that scientists were misinterpreting the data. These issues and the results of many experiments such as the wave-particle duality, the Lamb shift, anomalous magnetic moment of the electron, transition and decay lifetimes, experiments invoking interpretations of spooky action at a distance such as the Aspect experiment, entanglement, and double-slit-type experiments are shown to be absolutely predictable and physical in the context of a theory of classical quantum mechanics (CQM) derived from first principles [6-8]. Using the classical wave equation with the constraint of nonradiation based on Maxwell's equations, CQM gives closed form physical solutions for the electron in atoms, the free electron, and the free electron in superfluid helium which match the observations without requiring that the electron is divisible.

CLASSICAL QUANTUM THEORY OF THE ATOM BASED ON MAXWELL'S EQUATIONS

In this paper, the old view that the electron is a zero or one-dimensional point in an all-space probability wave function $\Psi(x)$ is not taken for granted. The theory of classical quantum mechanics (CQM), derived from first principles, must successfully and consistently apply physical laws on all scales [6-8]. Historically, the point at which QM broke with classical laws can be traced to the issue of nonradiation of the one electron atom that was addressed by Bohr with a postulate of stable orbits in defiance of the physics represented by Maxwell's equations [6-8]. Later physics was replaced by "pure mathematics" based on the notion of the inexplicable wave-particle duality nature of electrons which lead to the Schrödinger equation wherein the consequences of radiation predicted by Maxwell's equations was ignored. Ironically, both Bohr and Schrödinger used the electrostatic Coulomb potential of Maxwell's equations, but abandoned the electrodynamic laws. Physical laws may indeed be the root of the observations thought to be "purely quantum mechanical", and it may have been a mistake to make the assumption that Maxwell's electrodynamic equations must be rejected at the atomic level. Thus, in the present approach, the classical wave equation is solved with the constraint that a bound electron cannot radiate energy.

Thus, herein, derivations consider the electrodynamic effects of moving charges as well as the Coulomb potential, and the search is for a solution representative of the electron wherein there is acceleration of charge motion without radiation. The mathematical formulation for zero radiation based on Maxwell's equations follows from a derivation by Haus [13]. The function that describes the motion of the electron must not possess spacetime Fourier components that are synchronous with waves traveling at the speed of light. Similarly, nonradiation is demonstrated based on the electron's electromagnetic fields and the Poynting power vector.

In this paper, a summary of the results of CQM [6-8, 14-15] is presented that applies to explaining the behavior of free electrons in superfluid helium. Specifically, CQM gives closed form solutions for the atom including the stability of the $n = 1$ state and the instability of the excited states, the equation of the photon and electron in excited states, the equation of the free electron, and photon which predict the wave particle duality behavior of particles and light. The current and charge density functions of the electron may be directly physically interpreted. For example, spin angular momentum results from the motion of negatively charged mass moving systematically, and the equation for angular momentum, $\mathbf{r} \times \mathbf{p}$, can be applied directly to the wave function (a current density function) that describes the electron. The magnetic moment of a Bohr magneton, Stern Gerlach experiment, g factor, Lamb shift, resonant line width and shape, selection rules, correspondence principle, wave particle duality, excited states, reduced mass, rotational energies, and momenta, orbital and spin splitting, spin-orbital coupling, ionization energies of two electron atoms, and elastic electron scattering from helium atoms are derived in closed form equations based on Maxwell's equations. The calculations agree with experimental observations. Then, fractional principal quantum energy states are predicted for the free electron in superfluid helium which matches the observations without requiring that the electron is divisible.

ONE-ELECTRON ATOMS

One-electron atoms include the hydrogen atom, He^{+}, Li^{2+}, Be^{3+}, and so on. The mass-energy and angular momentum of the electron are constant; this requires that the equation of motion of the electron be temporally and spatially harmonic. Thus, the classical wave equation applies and

$$\left[\nabla^2 - \frac{1}{v^2}\frac{\partial^2}{\partial t^2}\right]\rho(r,\theta,\phi,t) = 0 \tag{2}$$

where $\rho(r,\theta,\phi,t)$ is the time dependent charge density function of the electron in time and space. In general, the wave equation has an infinite number of solutions. To arrive at the solution which represents the electron, a suitable boundary condition must be imposed. It is well known from experiments that each single atomic electron of a given isotope radiates to the same stable state. Thus, the physical boundary condition of nonradiation of the bound electron was imposed on the solution of the wave equation for the time dependent charge density function of the electron [6]. The condition for radiation by a moving point charge given by Haus [13] is that its spacetime Fourier transform does possess components that are synchronous with waves traveling at the speed of light. Conversely, it is proposed that the condition for nonradiation by an ensemble of moving point charges that comprises a current density function is

For non-radiative states, the current-density function must NOT possess spacetime Fourier components that are synchronous with waves traveling at the speed of light.

The time, radial, and angular solutions of the wave equation are separable. The motion is time harmonic with frequency ω_n. A constant angular function is a solution to the wave equation. Solutions of the Schrodinger wave equation comprising a radial function radiate according to Maxwell's equation as shown previously by application of Haus' condition [6]. In fact, it was found that any function which permitted radial motion gave rise to radiation. A radial function which does satisfy the boundary condition is a radial delta function

$$f(r) = \frac{1}{r^2}\delta(r - r_n) \tag{3}$$

This function defines a constant charge density on a spherical shell where $r_n = nr_1$, and Eq. (2) becomes the two-dimensional wave equation plus time with separable time and angular functions. Given time harmonic motion and a radial delta function, the relationship between an allowed radius and the electron wavelength is given by

$$2\pi r_n = \lambda_n \tag{4}$$

Using the observed de Broglie relationship for the electron mass where the coordinates are spherical,

$$\lambda_n = \frac{h}{p_n} = \frac{h}{m_e v_n} \tag{5}$$

and the magnitude of the velocity for *every* point on the orbitsphere is

$$v_n = \frac{\hbar}{m_e r_n} \tag{6}$$

The sum of the $\mathbf{L}_i$, the magnitude of the angular momentum of each infinitesimal point of the orbitsphere of mass m_i, must be constant. The constant is $\hbar$.

$$\sum |\mathbf{L}_i| = \sum |\mathbf{r} \times m_i \mathbf{v}| = m_e r_n \frac{\hbar}{m_e r_n} = \hbar \tag{7}$$

Thus, an electron is a spinning, two-dimensional spherical surface, called an *electron orbitsphere*, that can exist in a bound state at only specified distances from the nucleus as shown in Figure 1. The corresponding current function shown in Figure 2 which gives rise to the phenomenon of *spin* is derived in the "Spin Function" section.

Nonconstant functions are also solutions for the angular functions. To be a harmonic solution of the wave equation in spherical coordinates, these angular functions must be spherical harmonic functions [16]. A zero of the spacetime Fourier transform of the product function of two spherical harmonic angular functions, a time harmonic function, and an unknown radial function is sought. The solution for the radial function which satisfies the

boundary condition is also a delta function given by Eq. (3). Thus, bound electrons are described by a charge-density (mass-density) function which is the product of a radial delta function, two angular functions (spherical harmonic functions), and a time harmonic function.

$$\rho(r,\theta,\phi,t) = f(r)A(\theta,\phi,t) = \frac{1}{r^2}\delta(r - r_n)A(\theta,\phi,t); \qquad A(\theta,\phi,t) = Y(\theta,\phi)k(t) \tag{8}$$

In these cases, the spherical harmonic functions correspond to a traveling charge density wave confined to the spherical shell which gives rise to the phenomenon of orbital angular momentum. The orbital functions which modulate the constant "spin" function shown graphically in Figure 3 are given in the "Angular Functions" section.

SPIN FUNCTION

The orbitsphere spin function comprises a constant charge (current) density function with moving charge confined to a two-dimensional spherical shell. The current pattern of the orbitsphere spin function comprises an infinite series of correlated orthogonal great circle current loops wherein each point charge (current) density element moves time harmonically with constant angular velocity

$$\omega_n = \frac{\hbar}{m_e r_n^2} \tag{9}$$

The current pattern is generated over the surface by a series of nested rotations of two orthogonal great circle current loops where the coordinate axes rotate with the two orthogonal great circles. Half of the pattern is generated as the z-axis rotates to the negative z-axis during a 1st set of nested rotations. The mirror image, second half of the pattern is generated as the z-axis rotates back to its original direction during a 2nd set of nested rotations.

Point Current Density Elements on Great Circle Current Loop One:

$$\begin{bmatrix} x_1 \\ y_1 \\ z_1 \end{bmatrix} = \begin{bmatrix} \cos(\Delta\alpha) & -\sin^2(\Delta\alpha) & -\sin(\Delta\alpha)\cos(\Delta\alpha) \\ 0 & \cos(\Delta\alpha) & -\sin(\Delta\alpha) \\ \sin(\Delta\alpha) & \cos(\Delta\alpha)\sin(\Delta\alpha) & \cos^2(\Delta\alpha) \end{bmatrix} \begin{bmatrix} x_1' \\ y_1' \\ z_1' \end{bmatrix} \tag{10}$$

and $\Delta\alpha' = -\Delta\alpha$ replaces $\Delta\alpha$ for $\sum_{n=1}^{\frac{\sqrt{2}\pi}{\Delta\alpha}} \Delta\alpha = \sqrt{2}\pi$; $\sum_{n=1}^{\frac{\sqrt{2}\pi}{|\Delta\alpha'|}} |\Delta\alpha'| = \sqrt{2}\pi$

Point Current Density Elements on Great Circle Current Loop Two:

$$\begin{bmatrix} x_2 \\ y_2 \\ z_2 \end{bmatrix} = \begin{bmatrix} \cos(\Delta\alpha) & -\sin^2(\Delta\alpha) & -\sin(\Delta\alpha)\cos(\Delta\alpha) \\ 0 & \cos(\Delta\alpha) & -\sin(\Delta\alpha) \\ \sin(\Delta\alpha) & \cos(\Delta\alpha)\sin(\Delta\alpha) & \cos^2(\Delta\alpha) \end{bmatrix} \begin{bmatrix} x_2' \\ y_2' \\ z_2' \end{bmatrix} \tag{11}$$

and $\Delta\alpha' = -\Delta\alpha$ replaces $\Delta\alpha$ for $\sum_{n=1}^{\frac{\sqrt{2}\pi}{\Delta\alpha}} \Delta\alpha = \sqrt{2}\pi$; $\sum_{n=1}^{\frac{\sqrt{2}\pi}{|\Delta\alpha'|}} |\Delta\alpha'| = \sqrt{2}\pi$

The orbitsphere is given by reiterations of Eqs. (10) and (11). The output given by the non primed coordinates is the input of the next iteration corresponding to each successive nested rotation by the infinitesimal angle where the summation of the rotation about each of the x-axis and the y-axis is $\sum_{n=1}^{\frac{\sqrt{2}\pi}{\Delta\alpha}} \Delta\alpha = \sqrt{2}\pi$ (1st set) and $\sum_{n=1}^{\frac{\sqrt{2}\pi}{|\Delta\alpha'|}} |\Delta\alpha'| = \sqrt{2}\pi$ (2nd set). The current pattern corresponding to great circle current loop one and two shown with 8.49 degree increments of the infinitesimal angular variable $\Delta\alpha(\Delta\alpha')$ of Eqs. (10) and (11) is shown from the perspective of looking along the z-axis in Figure 2. The true orbitsphere current pattern is given as $\Delta\alpha(\Delta\alpha')$ approaches zero. This current pattern gives rise to the phenomenon corresponding to the spin quantum number of the electron.

ANGULAR FUNCTIONS

The time, radial, and angular solutions of the wave equation are separable. Also based on the radial solution, the angular charge and current-density functions of the electron, $A(\theta,\phi,t)$, must be a solution of the wave equation in two dimensions (plus time),

$$\left[\nabla^2 - \frac{1}{v^2}\frac{\partial^2}{\partial t^2}\right]A(\theta,\phi,t) = 0 \tag{12}$$

where $\rho(r,\theta,\phi,t) = f(r)A(\theta,\phi,t) = \frac{1}{r^2}\delta(r-r_n)A(\theta,\phi,t)$ and $A(\theta,\phi,t) = Y(\theta,\phi)k(t)$

$$\left[\frac{1}{r^2\sin\theta}\frac{\partial}{\partial\theta}\left(\sin\theta\frac{\partial}{\partial\theta}\right)_{r,\phi} + \frac{1}{r^2\sin^2\theta}\left(\frac{\partial^2}{\partial\phi^2}\right)_{r,\theta} - \frac{1}{v^2}\frac{\partial^2}{\partial t^2}\right]A(\theta,\phi,t) = 0 \tag{13}$$

where v is the linear velocity of the electron. The charge-density functions including the time-function factor are

$\ell = 0$

$$\rho(r,\theta,\phi,t) = \frac{e}{8\pi r^2}[\delta(r-r_n)]\left[Y_\ell^m(\theta,\phi) + Y_0^0(\theta,\phi)\right] \tag{14}$$

$\ell \neq 0$

$$\rho(r,\theta,\phi,t) = \frac{e}{4\pi r^2}[\delta(r-r_n)]\left[Y_0^0(\theta,\phi) + \mathrm{Re}\left\{Y_\ell^m(\theta,\phi)\left[1+e^{i\omega_n t}\right]\right\}\right] \tag{15}$$

$\mathrm{Re}\left\{Y_\ell^m(\theta,\phi)\left[1+e^{i\omega_n t}\right]\right\} = \mathrm{Re}\left[Y_\ell^m(\theta,\phi) + Y_\ell^m(\theta,\phi)e^{i\omega_n t}\right] = P_\ell^m(\cos\theta)\cos m\phi + P_\ell^m(\cos\theta)\cos(m\phi+\omega_n t)$ and $\omega_n = 0$ for $m = 0$.

ACCELERATION WITHOUT RADIATION

Nonradiation Based on Haus' Condition

The Fourier transform of the electron charge density function given by Eq. (8) is a solution of the three-dimensional wave equation in frequency space ($\mathbf{k},\omega$ *space*). Then the corresponding Fourier transform of the current density function $K(s,\Theta,\Phi,\omega)$ is given by multiplying by the constant angular frequency.

$$K(s,\Theta,\Phi,\omega) = 4\pi\omega_n \frac{\sin(2s_n r_n)}{2s_n r_n} \otimes 2\pi \sum_{\upsilon=1}^{n} \frac{(-1)^{\upsilon-1}(\pi\sin\Theta)^{2(\upsilon-1)}}{(\upsilon-1)!(\upsilon-1)!} \frac{\Gamma\left(\frac{1}{2}\right)\Gamma\left(\upsilon+\frac{1}{2}\right)}{(\pi\cos\Theta)^{2\upsilon+1}2^{\upsilon+1}} \frac{2\upsilon!}{(\upsilon-1)!} s^{-2\upsilon}$$
$$\otimes 2\pi \sum_{\upsilon=1}^{n} \frac{(-1)^{\upsilon-1}(\pi\sin\Phi)^{2(\upsilon-1)}}{(\upsilon-1)!(\upsilon-1)!} \frac{\Gamma\left(\frac{1}{2}\right)\Gamma\left(\upsilon+\frac{1}{2}\right)}{(\pi\cos\Phi)^{2\upsilon+1}2^{\upsilon+1}} \frac{2\upsilon!}{(\upsilon-1)!} s^{-2\upsilon} \frac{1}{4\pi}[\delta(\omega-\omega_n)+\delta(\omega+\omega_n)] \tag{16}$$

$\mathbf{s}_n \bullet \mathbf{v}_n = \mathbf{s}_n \bullet \mathbf{c} = \omega_n$ implies $r_n = \lambda_n$ Spacetime harmonics of $\frac{\omega_n}{c} = k$ or $\frac{\omega_n}{c}\sqrt{\frac{\varepsilon}{\varepsilon_o}} = k$ for which the Fourier transform of the current-density function is nonzero do not exist. Radiation due to charge motion does not occur in any medium when this boundary condition is met. (Nonradiation is also determined from the fields based on Maxwell's equations [6].)

Nonradiation Based on the Electron Electromagnetic Fields and the Poynting Power Vector

A point charge undergoing periodic motion accelerates and as a consequence radiates according to the Larmor formula:

$$P = \frac{1}{4\pi\varepsilon_0}\frac{2e^2}{3c^3}a^2 \tag{17}$$

where e is the charge, a is its acceleration, ε_0 is the permittivity of free space, and c is the speed of light. Although an accelerated *point* particle radiates, an *extended distribution* modeled as a superposition of accelerating charges does not have to radiate. An ensemble of charges, all oscillating at the same frequency, create a radiation pattern with a number of nodes. The same applies to current patterns in phased array antenna design [17]. It is possible to have an infinite number of charges oscillating in such as way as to cause destructive interference or nodes in all directions. In order to obtain the condition, if it exists, that the electron current distribution given by Eq. (25) must satisfy such that the electron does not radiate, the electromagnetic far field is determined from the current distribution. The vector potential in the Lorentz gauge satisfies

$$\nabla^2\mathbf{A} + \omega^2\mu_0\varepsilon_0\mathbf{A} = -\mu_0\mathbf{J} \tag{18}$$

where μ_0 is the permeability of free space, ω is the angular frequency of the time harmonic electron motion, $\mathbf{J}$ is the current of the electron, and $\mathbf{A}$ is the vector potential given by

$$\mathbf{A}(\mathbf{r}) = \frac{\mu_0}{4\pi}\int \frac{\mathbf{J}\left(\mathbf{r}', t-|\mathbf{r}-\mathbf{r}'|/c\right)}{|\mathbf{r}-\mathbf{r}'|}d^3r' \tag{19}$$

where the coordinates are shown in Figure 4. The magnetic field is given by

$$\mathbf{H} = \frac{1}{\mu_0}\nabla\times\mathbf{A} \tag{20}$$

The electric field is given by

$$\mathbf{E} = \frac{1}{j\omega\varepsilon_0}\nabla \times \mathbf{H} \tag{21}$$

The power density $S(t)$ is given by

$$S(t) = \mathbf{E} \times \mathbf{H} \tag{22}$$

The charge density functions of the electron orbitsphere in spherical coordinates plus time are given by Eqs. (14-15). For $\ell = 0$, the equipotential, uniform or constant charge density function (Eq. (14)) further comprises a current pattern given in the Spin Function section. It also corresponds to the nonradiative $n = 1$, $\ell = 0$ state of atomic hydrogen and to the spin function of the electron. The current density function is given by multiplying Eq. (14) by the constant angular velocity ω. There is acceleration without radiation. In this case, centripetal acceleration. A static charge distribution exists even though each point on the surface is accelerating along a great circle. Haus' condition predicts no radiation for the entire ensemble. The same result is trivially predicted from consideration of the fields and the radiated power. Since the current is not time dependent, the fields are given by

$$\nabla \times \mathbf{H} = \mathbf{J} \tag{23}$$

and

$$\nabla \times \mathbf{E} = 0 \tag{24}$$

which are the electrostatic and magnetostatic cases, respectively, with no radiation. Also see Daboul and Jensen [18].

The nonradiation condition given by Eq. (16) may be confirmed by determining the fields and the current distribution condition that is nonradiative based on Maxwell's equations. For $\ell \neq 0$, the charge-density functions including the time-function factor are given by Eqs. (15). In the cases that $m \neq 0$, Eq. (15) is a traveling charge density wave that moves on the surface of the orbitsphere about the z-axis and modulates the orbitsphere corresponding to $\ell = 0$. Since the charge is moving time harmonically about the z-axis with frequency ω_n and the current-density function is given by the time derivative of the charge-density function, the current-density function is given by the normalized product of the constant angular velocity and the charge-density function. The first current term of Eq. (15) is static. Thus, it is trivially nonradiative. The current due to the time dependent term is

$$
\begin{aligned}
\mathbf{J} &= \omega_n \frac{e}{4\pi r^2} N[\delta(r-r_n)]\mathrm{Re}\left\{Y_\ell^m(\theta,\phi)\left[1+e^{i\omega_n t}\right]\right\}\hat{\phi} \\
&= \omega_n \frac{e}{4\pi r^2} N[\delta(r-r_n)]\mathrm{Re}\left\{Y_\ell^m(\theta,\phi)+Y_\ell^m(\theta,\phi)e^{i\omega_n t}\right\}\hat{\phi} \\
&= \omega_n \frac{e}{4\pi r^2} N[\delta(r-r_n)]\left(P_\ell^m(\cos\theta)\cos m\phi + P_\ell^m(\cos\theta)e^{im\phi}e^{i\omega_n t}\right)\hat{\phi} \\
&= \omega_n \frac{e}{4\pi r^2} N[\delta(r-r_n)]\left(P_\ell^m(\cos\theta)\cos m\phi + P_\ell^m(\cos\theta)\cos\left(m\phi+\omega_n t\right)\right)\hat{\phi}
\end{aligned}
\tag{25}
$$

where N is the normalization constant. Let $r_n = R$ in Eq. (15). Using the coordinate designation shown in Figure 4, the vector potential due to the time dependent term is given by

$$
\mathbf{A}(\mathbf{r},t) = e\frac{\omega_n}{2\pi} m \frac{2\ell+1}{2R^2}\frac{\mu_0}{4\pi}\int_0^{2\pi}\int_0^{\pi}\int_0^{\infty} Y_\ell^m(\theta,\phi)\frac{e^{i\omega_n(t-|\mathbf{r}-\mathbf{r}'|/c)}}{|\mathbf{r}-\mathbf{r}'|}\hat{u}\times\hat{r}'\,\delta(r-R)r^2\sin\theta dr d\theta d\Phi \tag{26}
$$

$$
\mathbf{A}(\mathbf{r},t) = e\frac{\omega_n}{2\pi} m \frac{2\ell+1}{2R^2}\frac{\mu_0}{4\pi} e^{i\omega_n t}\hat{u}\times\int_0^{2\pi}\int_0^{\pi}\int_0^{\infty}\hat{r}'\,Y_\ell^m(\theta,\phi)\frac{e^{-ik|\mathbf{r}-\mathbf{r}'|}}{|\mathbf{r}-\mathbf{r}'|}\delta(r-R)r^2\sin\theta dr d\theta d\Phi \tag{27}
$$

where "^" denotes the unit vectors $\hat{\mathbf{u}} \equiv \dfrac{\mathbf{u}}{|\mathbf{u}|}$, and the current function is normalized. The expansion of the Green function given by Jackson [19] is

$$
\frac{e^{-ik|\mathbf{r}-\mathbf{r}'|}}{|\mathbf{r}-\mathbf{r}'|} = ik\sum_{\ell=0}^{\infty} j_\ell(kr_<)h_\ell^{(1)}(kr_>)\sum_{m=-\ell}^{\ell} Y_{\ell,m}^*(\theta',\phi')Y_{\ell,m}(\theta,\phi) \tag{28}
$$

where

$$
r_< \equiv \min(r,R), \qquad r_> \equiv \max(r,R) \tag{29}
$$

Since the modulation function $Y_{\ell,m}(\theta,\phi)$ is a traveling charge density wave that moves time harmonically on the surface of the orbitsphere about the z-axis with frequency ω_n, ϕ is a function of t. Substitution of Eq. (28) into Eq. (27) gives

$$
\mathbf{A}(\mathbf{r},t) = e\frac{\omega_n}{2\pi} m\left[\frac{2\ell+1}{2}\right]\frac{\mu_0}{4\pi}\int_0^{2\pi} e^{i(\omega_n t+m\phi)}\hat{u}\times\int_0^{\pi}\hat{r}ikj_\ell(kr_<)h_\ell^{(1)}(kr_>)\left(P_\ell^m(\cos\theta)\right)^2\sin\theta d\theta d\Phi \tag{30}
$$

$$
\mathbf{A}(\mathbf{r},t) = e\frac{m\omega_n}{2\pi}\frac{\mu_0}{4\pi}\int_0^{2\pi} e^{i\omega_n t}\hat{u}\times\hat{r}ikj_\ell(kr_<)h_\ell^{(1)}(kr_>)\cos(m\phi)d\Phi \tag{31}
$$

$$
\mathbf{A}(\mathbf{r},t) = e\frac{m\omega_n}{2\pi}\frac{\mu_0}{4\pi}\int_0^{vT_n} e^{i\omega_n t}\hat{u}\times\hat{r}ikj_\ell(kr_<)h_\ell^{(1)}(kr_>)\cos(mks(t))ds \tag{32}
$$

where $s(t)$ is the angular displacement of the rotation modulation function during one period T_n and v is the linear velocity in the $\hat{u}\times\hat{r}'$ direction. Thus,

$$
\mathbf{A}(\mathbf{r},t) = e\frac{\omega_n}{2\pi}\frac{\mu_0}{4\pi} i\left[e^{i\omega_n t}\hat{u}\times\hat{r}\right]j_\ell(kr_<)h_\ell^{(1)}(kr_>)\sin(mkvT_n) \tag{33}
$$

$$
\mathbf{A}(\mathbf{r},t) = e\frac{\omega_n}{2\pi}\frac{\mu_0}{4\pi} i\left[e^{i\omega_n t}\hat{u}\times\hat{r}\right]j_\ell(kr_<)h_\ell^{(1)}(kr_>)\sin(mks) \tag{34}
$$

In the case that k is the lightlike k^0, then $k = \omega_n / c$, and Eq. (34) vanishes for

$$
R = cT_n \tag{35}
$$

$$R T_n^{-1} = c \tag{36}$$

$$Rf = c \tag{37}$$

Thus,

$$s = vT_n = R = r_n = \lambda_n \tag{38}$$

which is identical to the Haus condition for nonradiation given by Eq. (16).

The electric and magnetic fields and the power density as a function of time are given by Eq.(34) and Eqs. (20-22). The spherical components of the fields, are defined by

$$E = E_r \hat{r} + E_\phi \hat{\phi} + E_\theta \hat{\theta} \tag{39}$$

where

$$\hat{\phi} = \frac{\hat{u} \times \hat{r}}{|\hat{u} \times \hat{r}|} = \frac{\hat{u} \times \hat{r}}{\sin\theta} \tag{40}$$

$$\hat{u} = \hat{z} = orbital\ axis \tag{41}$$

$$\hat{\theta} = \hat{\phi} \times \hat{r} \tag{42}$$

The fields inside of the electron orbitsphere ($r < R$) are

$$E_r = E_\theta = B_\phi = 0 \tag{43}$$

$$E_\phi = -\sqrt{\frac{\mu_0}{\varepsilon_0}} ke \frac{\omega_n}{2\pi} \frac{1}{4\pi} h_\ell^{(1)}(kR) j_\ell(kr) \sin(mks) \sin\theta e^{i\omega_n t} \tag{44}$$

$$H_r = 2e \frac{\omega_n}{2\pi} \frac{1}{4\pi} ik \frac{h_\ell^{(1)}(kR)}{kr} j_\ell(kr) \sin(mks) \cos\theta e^{i\omega_n t} \tag{45}$$

$$H_\theta = -2e \frac{\omega_n}{2\pi} \frac{1}{4\pi} ik \frac{h_\ell^{(1)}(kR)}{kr} \frac{d}{dkr}\left(krj_\ell(kr)\right) \sin(mks) \sin\theta e^{i\omega_n t} \tag{46}$$

The fields outside of the electron orbitsphere ($r > R$) are

$$E_r = E_\theta = B_\phi = 0 \tag{47}$$

$$E_\phi = -\sqrt{\frac{\mu_0}{\varepsilon_0}} ke \frac{\omega_n}{2\pi} \frac{1}{4\pi} j_\ell(kR) h_\ell^{(1)}(kr) \sin(mks) \sin\theta e^{i\omega_n t} \tag{48}$$

$$H_r = 2e \frac{\omega_n}{2\pi} \frac{1}{4\pi} ik \frac{j_\ell(kR)}{kr} h_\ell^{(1)}(kr) \sin(mks) \cos\theta e^{i\omega_n t} \tag{49}$$

$$H_\theta = -2e \frac{\omega_n}{2\pi} \frac{1}{4\pi} ik \frac{j_\ell(kR)}{kr} \frac{d}{dkr}\left(krh_\ell^{(1)}(kr)\right) \sin(mks) \sin\theta e^{i\omega_n t} \tag{50}$$

The power density $S(t)$ is given by substitution of Eqs. (48) and (50) into Eq. (22).

$$S(t) = -\sqrt{\frac{\mu_0}{\varepsilon_0}} ke \frac{\omega_n}{2\pi} \frac{1}{4\pi} j_\ell(kR) h_\ell^{(1)}(kr) \sin(mks) \sin\theta e^{i\omega_n t} \hat{\phi}$$
$$\times -2e \frac{\omega_n}{2\pi} \frac{1}{4\pi} ik \frac{j_\ell(kR)}{kr} \frac{d}{dkr} \left(kr h_\ell^{(1)}(kr)\right) \sin(mks) \sin\theta e^{i\omega_n t} \hat{\theta} \quad (51)$$

$$S(t) = ik^2 2 \sqrt{\frac{\mu_0}{\varepsilon_0}} \left(\frac{\omega_n}{2\pi} \frac{e}{4\pi}\right)^2 \frac{\left(j_\ell(kR)\right)^2}{kr} h_\ell^{(1)}(kr) \frac{d}{dkr} \left(kr h_\ell^{(1)}(kr)\right) \sin^2(mks) \sin^2\theta e^{i2\omega_n t} \hat{r} \quad (52)$$

For the condition given by Eq. (38), the power density as a function of time $S(t)$ is zero. *There is no radiation.*

MAGNETIC FIELD EQUATIONS OF THE ELECTRON

The orbitsphere is a shell of negative charge current comprising correlated charge motion along great circles. For $\ell = 0$, the orbitsphere gives rise to a magnetic moment of 1 Bohr magneton [20].

$$\mu_B = \frac{e\hbar}{2m_e} = 9.274 \times 10^{-24} JT^{-1}, \quad (53)$$

The magnetic field of the electron shown in Figure 5 is given by

$$\mathbf{H} = \frac{e\hbar}{m_e r_n^3} (\mathbf{i}_r \cos\theta - \mathbf{i}_\theta \sin\theta) \quad \text{for } r < r_n \quad (54)$$

$$\mathbf{H} = \frac{e\hbar}{2m_e r^3} (\mathbf{i}_r 2\cos\theta - \mathbf{i}_\theta \sin\theta) \quad \text{for } r > r_n \quad (55)$$

The energy stored in the magnetic field of the electron is

$$E_{mag} = \frac{1}{2} \mu_o \int_0^{2\pi} \int_0^{\pi} \int_0^{\infty} H^2 r^2 \sin\theta dr d\theta d\Phi \quad (56)$$

$$E_{mag\,\text{total}} = \frac{\pi \mu_o e^2 \hbar^2}{m_e^2 r_1^3} \quad (57)$$

STERN-GERLACH EXPERIMENT

The Stern-Gerlach experiment implies a magnetic moment of one Bohr magneton and an associated angular momentum quantum number of 1/2. Historically, this quantum number is called the spin quantum number, s ($s = \frac{1}{2}$; $m_s = \pm\frac{1}{2}$). The superposition of the vector projection of the orbitsphere angular momentum on to an axis **S** that precesses about the z-axis called the spin axis at an angle of $\theta = \frac{\pi}{3}$ and an angle of $\phi = \pi$ with respect to $\langle \mathbf{L}_{xy} \rangle_{\Sigma \Delta \alpha}$ is

$$\mathbf{S} = \pm\sqrt{\frac{3}{4}}\hbar \quad (58)$$

S rotates about the z-axis at the Larmor frequency. $\langle \mathbf{S}_z \rangle$, the time averaged projection of the orbitsphere angular momentum onto the axis of the applied magnetic field is

$$\langle \mathbf{L}_z \rangle_{\Sigma \Delta a} \pm \frac{\hbar}{2}. \tag{59}$$

ELECTRON g FACTOR

Conservation of angular momentum of the orbitsphere permits a discrete change of its "kinetic angular momentum" ($\mathbf{r} \times m\mathbf{v}$) by the applied magnetic field of $\frac{\hbar}{2}$, and concomitantly the "potential angular momentum" ($\mathbf{r} \times e\mathbf{A}$) must change by $-\frac{\hbar}{2}$.

$$\Delta \mathbf{L} = \frac{\hbar}{2} - \mathbf{r} \times e\mathbf{A} \tag{60}$$

$$= \left[\frac{\hbar}{2} - \frac{e\phi}{2\pi}\right]\hat{z} \tag{61}$$

In order that the change of angular momentum, $\Delta \mathbf{L}$, equals zero, ϕ must be $\Phi_0 = \frac{h}{2e}$, the magnetic flux quantum. The magnetic moment of the electron is parallel or antiparallel to the applied field only. During the spin-flip transition, power must be conserved. Power flow is governed by the Poynting power theorem,

$$\nabla \bullet (\mathbf{E} \times \mathbf{H}) = -\frac{\partial}{\partial t}\left[\frac{1}{2}\mu_o \mathbf{H} \bullet \mathbf{H}\right] - \frac{\partial}{\partial t}\left[\frac{1}{2}\varepsilon_o \mathbf{E} \bullet \mathbf{E}\right] - \mathbf{J} \bullet \mathbf{E} \tag{62}$$

Eq. (63) gives the total energy of the flip transition which is the sum of the energy of reorientation of the magnetic moment (1st term), the magnetic energy (2nd term), the electric energy (3rd term), and the dissipated energy of a fluxon treading the orbitsphere (4th term), respectively,

$$\Delta E_{mag}^{spin} = 2\left(1 + \frac{\alpha}{2\pi} + \frac{2}{3}\alpha^2\left(\frac{\alpha}{2\pi}\right) - \frac{4}{3}\left(\frac{\alpha}{2\pi}\right)^2\right)\mu_B B \tag{63}$$

$$\Delta E_{mag}^{spin} = g\mu_B B \tag{64}$$

where the stored magnetic energy corresponding to the $\frac{\partial}{\partial t}\left[\frac{1}{2}\mu_o \mathbf{H} \bullet \mathbf{H}\right]$ term increases, the stored electric energy corresponding to the $\frac{\partial}{\partial t}\left[\frac{1}{2}\varepsilon_o \mathbf{E} \bullet \mathbf{E}\right]$ term increases, and the $\mathbf{J} \bullet \mathbf{E}$ term is dissipative. The spin-flip transition can be considered as involving a magnetic moment of g times that of a Bohr magneton. The g factor is redesignated the fluxon g factor as opposed to

the anomalous g factor. The calculated value of $\frac{g}{2}$ is 1.001 159 652 137. The experimental value [21] of $\frac{g}{2}$ is 1.001 159 652 188(4).

SPIN AND ORBITAL PARAMETERS

The total function that describes the spinning motion of each electron orbitsphere is composed of two functions. One function, the spin function, is spatially uniform over the orbitsphere, spins with a quantized angular velocity, and gives rise to spin angular momentum. The other function, the modulation function, can be spatially uniform—in which case there is no orbital angular momentum and the magnetic moment of the electron orbitsphere is one Bohr magneton—or not spatially uniform—in which case there is orbital angular momentum. The modulation function also rotates with a quantized angular velocity.

The spin function of the electron corresponds to the nonradiative $n = 1$, $\ell = 0$ state of atomic hydrogen which is well known as an s state or orbital. (See Figure 1 for the charge function and Figure 2 for the current function.) In cases of orbitals of heavier elements and excited states of one electron atoms and atoms or ions of heavier elements with the ℓ quantum number not equal to zero and which are not constant as given by Eq. (14), the constant spin function is modulated by a time and spherical harmonic function as given by Eq. (15) and shown in Figure 3. The modulation or traveling charge density wave corresponds to an orbital angular momentum in addition to a spin angular momentum. These states are typically referred to as p, d, f, etc. orbitals. Application of Haus's [13] condition also predicts nonradiation for a constant spin function modulated by a time and spherically harmonic orbital function. There is acceleration without radiation as also shown in the Nonradiation Based on the Electron Electromagnetic Fields and the Poynting Power Vector Section. (Also see Abbott and Griffiths and Goedecke [22-23]). However, in the case that such a state arises as an excited state by photon absorption, it is radiative due to a radial dipole term in its current density function since it possesses spacetime Fourier Transform components synchronous with waves traveling at the speed of light [13]. (See Instability of Excited States" section.)

Moment of Inertia and Spin and Rotational Energies

$$\mathbf{\ell} = 0$$

$$I_z = I_{spin} = \frac{m_e r_n^2}{2} \tag{65}$$

$$L_z = I\omega \mathbf{i}_z = \pm\frac{\hbar}{2} \tag{66}$$

$$E_{rotational} = E_{rotational,\ spin} = \frac{1}{2}\left[I_{spin}\left(\frac{\hbar}{m_e r_n^{\,2}}\right)^2\right] = \frac{1}{2}\left[\frac{m_e r_n^{\,2}}{2}\left(\frac{\hbar}{m_e r_n^{\,2}}\right)^2\right] = \frac{1}{4}\left[\frac{\hbar^2}{2I_{spin}}\right] \tag{67}$$

$\ell \neq 0$

$$I_{orbital} = m_e r_n^{\,2}\left[\frac{\ell(\ell+1)}{\ell^2+\ell+1}\right]^{\frac{1}{2}} \tag{68}$$

$$L_z = m\hbar \tag{69}$$

$$L_{z\ total} = L_{z\ spin} + L_{z\ orbital} \tag{70}$$

$$E_{rotational,\ orbital} = \frac{\hbar^2}{2I}\left[\frac{\ell(\ell+1)}{\ell^2+2\ell+1}\right] \tag{71}$$

$$T = \frac{\hbar^2}{2m_e r_n^2} \tag{72}$$

$$\left\langle E_{rotational,\ orbital}\right\rangle = 0 \tag{73}$$

From Eq. (73), the time average rotational energy is zero; thus, the principal levels are degenerate except when a magnetic field is applied.

FORCE BALANCE EQUATION

The radius of the nonradiative ($n = 1$) state is solved using the electromagnetic force equations of Maxwell relating the charge and mass density functions wherein the angular momentum of the electron is given by Planck's constant bar. The reduced mass arises naturally from an electrodynamic interaction between the electron and the proton.

$$\frac{m_e}{4\pi r_1^{\,2}}\frac{v_1^{\,2}}{r_1} = \frac{e}{4\pi r_1^{\,2}}\frac{Ze}{4\pi\varepsilon_o r_1^{\,2}} - \frac{1}{4\pi r_1^{\,2}}\frac{\hbar^2}{mr_n^{\,3}} \tag{74}$$

$$r_1 = \frac{a_H}{Z} \tag{75}$$

ENERGY CALCULATIONS

From Maxwell's equations, the potential energy V, kinetic energy T, electric energy or binding energy E_{ele} are

$$V = \frac{-Ze^2}{4\pi\varepsilon_o r_1} = \frac{-Z^2e^2}{4\pi\varepsilon_o a_H} = -Z^2\ X\ 4.3675\ X\ 10^{-18}\ J = -Z^2\ X\ 27.2\ eV \tag{76}$$

$$T = \frac{Z^2e^2}{8\pi\varepsilon_o a_H} = Z^2\ X\ 13.59\ eV \tag{77}$$

$$T = E_{ele} = -\frac{1}{2}\varepsilon_o \int_{\infty}^{r_1} \mathbf{E}^2 dv \quad \text{where } \mathbf{E} = -\frac{Ze}{4\pi\varepsilon_o r^2}. \tag{78}$$

$$E_{ele} = -\frac{Z^2 e^2}{8\pi\varepsilon_o a_H} = -Z^2 \, X \, 2.1786 \, X 10^{-18} \, J = -Z^2 \, X \, 13.598 \, eV \tag{79}$$

The calculated Rydberg constant is $10,967,758\ m^{-1}$; the experimental Rydberg constant is $10,967,758\ m^{-1}$[1].

---

[1] The theories of Bohr, Schrödinger, and presently CQM all give the identical equation for the principal energy levels of the hydrogen atom.

$$E_{ele} = -\frac{Z^2 e^2}{8\pi\varepsilon_o n^2 a_H} = -\frac{Z^2}{n^2} \, X \, 2.1786 \, X 10^{-18} \, J = -Z^2 \, X \, \frac{13.598}{n^2} \, eV \tag{FN1.1}$$

In CQM, the two dimensional wave equation is solved for the charge density function of the electron. And, the Fourier transform of the charge density function is a solution of the three dimensional wave equation in frequency (k,ω) space. Whereas, the Schrödinger equation solutions are three dimensional in spacetime. The energy is given by

$$\int_{-\infty}^{\infty} \psi H \psi dv = E \int_{-\infty}^{\infty} \psi^2 dv; \tag{FN1.2}$$

$$\int_{-\infty}^{\infty} \psi^2 dv = 1 \tag{FN1.3}$$

Thus,

$$\int_{-\infty}^{\infty} \psi H \psi dv = E \tag{FN1.4}$$

In the case that the potential energy of the Hamiltonian, H, is a constant times the wavenumber, the Schrödinger equation is the well known Bessel equation. Then with one of the solutions for ψ, Eq. (FN1.4) is equivalent to an inverse Fourier transform. According to the duality and scale change properties of Fourier transforms, the energy equation of CQM and that of quantum mechanics are identical, the energy of a radial Dirac delta function of radius equal to an integer multiple of the radius of the hydrogen atom (Eq. (FN1.1)). And, Bohr obtained the same energy formula by postulating nonradiative states with angular momentum

$$L_z = m\hbar \tag{FN1.5}$$

and solving the energy equation classically.

The mathematics for all three theories converge to Eq. (FN1.1). However, the physics is quite different. Only CQM is derived from first principles, and the mathematical relationship of CQM and QM is based on the Fourier transform of the radial function. CQM requires that the electron is real and physically confined to a two dimensional surface which corresponds to a solution of the two-dimensional wave equation plus time. The corresponding Fourier transform is a wave over all space which is a solution of the three dimensional wave equation (e.g. the Schrödinger equation). In essence QM may be considered as a theory dealing with the Fourier transform of an electron rather than the physical electron. By Parseval's theorem, the energies may be equivalent, but the quantum mechanical case is nonphysical—only mathematical. Classical revisions may transform Schrödinger's and Heisenberg's quantum theory into what is termed a *classical quantum theory* such that physical descriptions result.

EXCITED STATES

CQM gives closed form solutions for the resonant photons and excited state electron functions. The angular momentum of the photon given by

$$\mathbf{m} = \frac{1}{8\pi}\mathrm{Re}\left[\mathbf{r} \times (\mathbf{E} \times \mathbf{B}^*)\right] = \hbar \tag{80}$$

is conserved [24]. The change in angular velocity of the electron is equal to the angular frequency of the resonant photon. The energy is given by Planck's equation. The predicted energies, Lamb shift, hyperfine structure, resonant line shape, line width, selection rules, etc. are in agreement with observation.

The orbitsphere is a dynamic spherical resonator cavity which traps photons of discrete frequencies. The relationship between an allowed radius and the "photon standing wave" wavelength is

$$2\pi r = n\lambda \tag{81}$$

where n is an integer. The relationship between an allowed radius and the electron wavelength is

$$2\pi(nr_1) = 2\pi r_n = n\lambda_1 = \lambda_n \tag{82}$$

where $n = 1,2,3,4,\ldots$. The radius of an orbitsphere increases with the absorption of electromagnetic energy. The radii of excited states are solved using the electromagnetic force equations of Maxwell relating the field from the charge of the proton, the electric field of the photon, and charge and mass density functions of the electron wherein the angular momentum of the electron is given by Planck's constant bar (Eq. (74)). The solutions to Maxwell's equations for modes that can be excited in the orbitsphere resonator cavity give rise to four quantum numbers, and the energies of the modes are the experimentally known hydrogen spectrum. The relationship between the electric field equation and the "trapped photon" source charge-density function is given by Maxwell's equation in two dimensions.

$$\mathbf{n} \bullet \left(\mathbf{E}_i - \mathbf{E}_2\right) = \frac{\sigma}{\varepsilon_0} \tag{83}$$

The photon standing electromagnetic wave is phase matched with the electron

$$\mathbf{E}_{r\,photon\;n,l,m} = \frac{e(na_H)^\ell}{4\pi\varepsilon_o}\frac{1}{r^{(\ell+2)}}\left[-Y_0^0(\theta,\phi) + \frac{1}{n}\left[Y_0^0(\theta,\phi) + \mathrm{Re}\left\{Y_\ell^m(\theta,\phi)\left[1 + e^{i\omega_n t}\right]\right\}\right]\right]\delta(r - r_n) \tag{84}$$

$\omega_n = 0$ *for* $m = 0$

$\ell = 1,2,\ldots,n-1$

$m = -\ell, -\ell+1,\ldots,0,\ldots,+\ell$

$$\mathbf{E}_{r\,total} = \frac{e}{4\pi\varepsilon_o r^2} + \frac{e(na_H)^\ell}{4\pi\varepsilon_o}\frac{1}{r^{(\ell+2)}}\left[-Y_0^0(\theta,\phi) + \frac{1}{n}\left[Y_0^0(\theta,\phi) + \mathrm{Re}\left\{Y_\ell^m(\theta,\phi)\left[1 + e^{i\omega_n t}\right]\right\}\right]\right]\delta(r - r_n)$$

(85)

$\omega_n = 0$ for $m = 0$

For $r = na_H$ and $m = 0$, the total radial electric field is

$$\mathbf{E}_{r\,total} = \frac{1}{n}\frac{e}{4\pi\varepsilon_o\left(na_H\right)^2} \tag{86}$$

The energy of the photon which excites a mode in the electron spherical resonator cavity from radius a_H to radius na_H is

$$E_{photon} = \frac{e^2}{8\pi\varepsilon_o a_H}\left[1 - \frac{1}{n^2}\right] = h\nu = \hbar\omega \tag{87}$$

The change in angular velocity of the orbitsphere for an excitation from $n = 1$ to $n = n$ is

$$\Delta\omega = \frac{\hbar}{m_e\left(a_H\right)^2} - \frac{\hbar}{m_e\left(na_H\right)^2} = \frac{\hbar}{m_e\left(a_H\right)^2}\left[1 - \frac{1}{n^2}\right] \tag{88}$$

The kinetic energy change of the transition is

$$\frac{1}{2}m_e(\Delta v)^2 = \frac{e^2}{8\pi\varepsilon_0 a_H}\left[1 - \frac{1}{n^2}\right] = \hbar\omega \tag{89}$$

The change in angular velocity of the electron orbitsphere is identical to the angular velocity of the photon necessary for the excitation, ω_{photon}. The *correspondence principle holds*. It can be demonstrated that the resonance condition between these frequencies is to be satisfied in order to have a net change of the energy field [25].

ORBITAL AND SPIN SPLITTING

The ratio of the square of the angular momentum, M^2, to the square of the energy, U^2, for a pure (ℓ, m) multipole is [26]

$$\frac{M^2}{U^2} = \frac{m^2}{\omega^2} \tag{90}$$

The magnetic moment is defined as

$$\mu = \frac{\text{charge x angular momentum}}{\text{2 x mass}} \tag{91}$$

The radiation of a multipole of order (ℓ, m) carries $m\hbar$ units of the z component of angular momentum per photon of energy $\hbar\omega$. Thus, the z component of the angular momentum of the corresponding excited state electron orbitsphere is

$$L_z = m\hbar \tag{92}$$

Therefore,

$$\mu_z = \frac{em\hbar}{2m_e} = m\mu_B \tag{93}$$

where μ_B is the Bohr magneton. The orbital splitting energy is

$$E_{mag}^{orb} = m\mu_B B \tag{94}$$

The spin and orbital splitting energies superimpose; thus, the principal excited state energy levels of the hydrogen atom are split by the energy $E_{mag}^{spin\,orb}$.

$$E_{mag}^{spin\,orb} = m\frac{e\hbar}{2m_e}B + m_s g\frac{e\hbar}{m_e}B \text{ where} \tag{95}$$

$$n = 2,3,4,\ldots$$

$$\ell = 1,2,\ldots,n-1$$

$$m = -\ell,-\ell+1,\ldots,0,\ldots,+\ell$$

$$m_s = \pm\frac{1}{2}$$

For the electric dipole transition, the selection rules are

$$\Delta n = 0,\pm 1$$
$$\Delta m_s = 0 \tag{96}$$

RESONANT LINE SHAPE AND LAMB SHIFT

The spectroscopic linewidth shown in Figure 6 arises from the classical rise-time band-width relationship, and the Lamb Shift is due to conservation of energy and linear momentum and arises from the radiation reaction force between the electron and the photon. It follows from the Poynting power theorem with spherical radiation that the transition probabilities are given by the ratio of power and the energy of the transition [27]. The transition probability in the case of the electric multipole moment is

$$\frac{1}{\tau} = \frac{power}{energy} \tag{97}$$

$$\frac{1}{\tau} = \frac{\left[\frac{2\pi c}{\left[(2\ell+1)!!\right]^2}\left(\frac{\ell+1}{\ell}\right)k^{2\ell+1}\left|Q_{\ell m}+Q_{\ell m}\right|^2\right]}{[\hbar\omega]} = 2\pi\left(\frac{e^2}{h}\right)\sqrt{\frac{\mu_0}{\varepsilon_0}}\frac{2\pi}{\left[(2\ell+1)!!\right]^2}\left(\frac{\ell+1}{\ell}\right)\left(\frac{3}{\ell+3}\right)^2\left(kr_n\right)^{2\ell}\omega \tag{98}$$

$$\mathbf{E}(\omega) \propto \int_0^\infty e^{-\alpha t}e^{-i\omega t}dt = \frac{1}{\alpha - i\omega} \tag{99}$$

The relationship between the rise-time and the band-width for exponential decay is

$$\tau\Gamma = \frac{1}{\pi} \tag{100}$$

The energy radiated per unit frequency interval is

$$\frac{dI(\omega)}{d\omega} = I_0\frac{\Gamma}{2\pi}\frac{1}{\left(\omega-\omega_0-\Delta\omega\right)^2+\left(\Gamma/2\right)^2} \tag{101}$$

LAMB SHIFT

The Lamb Shift of the ${}^2P_{1/2}$ state of the hydrogen atom is due to conservation of linear momentum of the electron, atom, and photon. The electron component is

$$\Delta f = \frac{\Delta\omega}{2\pi} = \frac{E_{h\upsilon}}{h} = 3\frac{\left(E_{h\upsilon}\right)^2}{h2m_e c^2} = 1052\ MHz \tag{102}$$

where $E_{h\upsilon}$ is

$$E_{h\nu} = 13.6\left(1-\frac{1}{n^2}\right)\frac{1}{\left|X_{\ell m}\right|^2_{\ell=1}} - h\Delta f \tag{103}$$

$$E_{h\nu} = 13.6\left(1-\frac{1}{n^2}\right)\frac{3}{8\pi} - h\Delta f \tag{104}$$

$$h\Delta f <<< 1 \tag{105}$$

Therefore,

$$E_{h\nu} = 13.6\left(1-\frac{1}{n^2}\right)\frac{3}{8\pi} \tag{106}$$

The atom component is

$$\Delta f = \frac{\Delta\omega}{2\pi} = \frac{E_{h\upsilon}}{h} = \frac{1}{2}\frac{\left(E_{h\upsilon}\right)^2}{2m_H c^2} = 6.5\ MHz \tag{107}$$

The sum of the components is

$$\Delta f = 1052\ MHz + 6.5\ MHz = 1058.5\ MHz \tag{108}$$

The experimental Lamb Shift is 1058 MHz.

SPIN-ORBITAL COUPLING

The electron's motion in the hydrogen atom is always perpendicular to its radius; consequently, as shown by Eq. (7), the electron's angular momentum of $\hbar$ is invariant. The angular momentum of the photon given in the Photon Equations section is $\mathbf{m} = \frac{1}{8\pi}\mathrm{Re}[\mathbf{r}\times(\mathbf{E}\times\mathbf{B}^*)] = \hbar$. It is conserved for the solutions for the resonant photons and excited state electron functions given in the Excited States section and the Photon Equations section. Thus, the electrodynamic angular momentum and the inertial angular momentum are matched such that the correspondence principle holds. It follows from the principle of conservation of angular momentum that $\frac{e}{m_e}$ of Eq. (53) is invariant as shown previously [6].

In the case of spin-orbital coupling, the invariant $\hbar$ of spin angular momentum and orbital angular momentum each give rise to a corresponding invariant magnetic moment of a Bohr magneton, and their corresponding energies superimpose as given in the Orbital and Spin Splitting section. The interaction of the two magnetic moments gives rise to a relativistic spin-

orbital coupling energy. The vector orientations of the momenta must be considered as well as the condition that flux must be linked by the electron in units of the magnetic flux quantum in order to conserve the invariant electron angular momentum of $\hbar$. The energy may be calculated with the additional conditions of the invariance of the electron's charge and mass to charge ratio $\frac{e}{m_e}$.

As shown in the Electron g Factor section (Eqs. (60-64)), flux must be linked by the electron orbitsphere in units of the magnetic flux quantum. The maximum projection of the spin angular momentum of the electron onto an axis given by Eq. (58) is $\sqrt{\frac{3}{4}}\hbar$. Then, using the magnetic energy term of Eq. (63), the spin-orbital coupling energy $E_{s/o}$ is given by

$$E_{s/o} = 2\frac{\alpha}{2\pi}\left(\frac{e\hbar}{2m_e}\right)\frac{\mu_0 e\hbar}{2(2\pi m_e)\left(\frac{r}{2\pi}\right)^3}\sqrt{\frac{3}{4}} = \frac{\alpha\pi\mu_0 e^2\hbar^2}{m_e^2 r^3}\sqrt{\frac{3}{4}} \tag{109}$$

In the case that $n = 2$, the radius given by Eq. (82) is $r = 2a_0$. The predicted energy difference between the ${}^2P_{3/2}$ and ${}^2P_{1/2}$ levels of the hydrogen atom, $E_{s/o}$, given by Eq. (109) is

$$E_{s/o} = \frac{\alpha\pi\mu_0 e^2\hbar^2}{8m_e^2 a_0^3}\sqrt{\frac{3}{4}} \tag{110}$$

wherein $\ell = 1$ and both levels are equivalently Lamb shifted. Using Eqs. (183-184), $E_{s/o}$ may be expressed in terms of the mass energy of the electron.

$$E_{s/o} = \frac{\alpha^5(2\pi)^2}{8}m_e c^2\sqrt{\frac{3}{4}} \tag{111}$$

The energy from Eq. (109) called the fine structure splitting is $4.51908\,X\,10^{-5}\ eV$ corresponding to a frequency of 10,934.3 MHz or a wavelength of about 2.74 cm. The ${}^2P_{3/2}$ and ${}^2P_{1/2}$ levels are also split by spin-nuclear and orbital-nuclear coupling. The experimental hyperfine structure transition frequencies for the ${}^2P_{3/2}$ and ${}^2P_{1/2}$ levels are 23.7 MHz and 59.19 MHz, respectively. ${}^2P_{3/2}$—${}^2P_{1/2}$ transitions occur between hyperfine levels; thus, the transition energy is the sum of the fine structure and the corresponding hyperfine energy. The calculated ${}^2P_{3/2}$—${}^2P_{1/2}$ transition frequency including a transition between hyperfine levels is 10,975.7 MHz. The large natural widths of the hydrogen $2p$ levels limits the experimental accuracy. The experimental value of the ${}^2P_{3/2}$—${}^2P_{1/2}$ transition frequency is 10,969.1 MHz.

INSTABILITY OF EXCITED STATES

For the excited energy states of the hydrogen atom, σ_{photon}, the two dimensional surface charge due to the "trapped photons" at the electron orbitsphere, given by Eq. (83) and Eq. (84) is

$$\sigma_{photon} = \frac{e}{4\pi(r_n)^2}\left[Y_0^0(\theta,\phi) - \frac{1}{n}\left[Y_0^0(\theta,\phi) + \mathrm{Re}\left\{ Y_\ell^m(\theta,\phi)\left[1 + e^{i\omega_n t}\right]\right\}\right]\right]\delta(r - r_n) \tag{112}$$

where $n = 2,3,4,\ldots,$. Whereas, $\sigma_{electron}$, the two dimensional surface charge of the electron orbitsphere given by Eq. (15) is

$$\sigma_{electron} = \frac{-e}{4\pi(r_n)^2}\left[Y_0^0(\theta,\phi) + \mathrm{Re}\left\{ Y_\ell^m(\theta,\phi)\left[1 + e^{i\omega_n t}\right]\right\}\right]\delta(r - r_n) \tag{113}$$

The superposition of σ_{photon} (Eq. (112)) and $\sigma_{electron}$ is equivalent to the sum of a radial electric dipole represented by a doublet function and a radial electric monopole represented by a delta function.

$\sigma_{photon} + \sigma_{electron} =$

$$\frac{e}{4\pi(r_n)^2}\left[Y_0^0(\theta,\phi)\dot{\delta}(r - r_n) - \frac{1}{n}Y_0^0(\theta,\phi)\delta(r - r_n) - \left(1 + \frac{1}{n}\right)\left[\mathrm{Re}\left\{ Y_\ell^m(\theta,\phi)\left[1 + e^{i\omega_n t}\right]\right\}\right]\delta(r - r_n)\right] \tag{114}$$

where $n = 2,3,4,\ldots,$. Due to the radial doublet, excited states are radiative since spacetime harmonics of $\frac{\omega_n}{c} = k$ or $\frac{\omega_n}{c}\sqrt{\frac{\varepsilon}{\varepsilon_o}} = k$ do exist for which the spacetime Fourier transform of the current density function is nonzero.

PHOTON EQUATIONS

The time-averaged angular-momentum density, $\mathbf{m}$, of an emitted photon is

$$\mathbf{m} = \frac{1}{8\pi}\mathrm{Re}[\mathbf{r} \times (\mathbf{E} \times \mathbf{B}^*)] = \hbar \tag{115}$$

A linearly polarized photon orbitsphere is generated from two orthogonal great circle field lines shown in Figure 7 rather than two great circle current loops as in the case of the electron spin function. The right-handed circularly polarized photon orbitsphere shown in Figure 8 corresponds to the case wherein the summation of the rotation about each of the x-axis and the y-axis is $\sum_{n=1}^{\frac{\sqrt{2}\pi}{\Delta\alpha}} \Delta\alpha = \sqrt{2}\pi$, and the mirror image left-handed circularly polarized photon orbitsphere corresponds to the case wherein the summation of the rotation about each of the x-axis and the y-axis is $\sum_{n=1}^{\frac{\sqrt{2}\pi}{|\Delta\alpha'|}} |\Delta\alpha'| = \sqrt{2}\pi$.

Nested Set of Great Circle Field Lines Generates the Photon Function

H Field:

$$\begin{bmatrix} x_1 \\ y_1 \\ z_1 \end{bmatrix} = \begin{bmatrix} \cos(\Delta\alpha) & -\sin^2(\Delta\alpha) & -\sin(\Delta\alpha)\cos(\Delta\alpha) \\ 0 & \cos(\Delta\alpha) & -\sin(\Delta\alpha) \\ \sin(\Delta\alpha) & \cos(\Delta\alpha)\sin(\Delta\alpha) & \cos^2(\Delta\alpha) \end{bmatrix} \begin{bmatrix} x_1' \\ y_1' \\ z_1' \end{bmatrix} \tag{116}$$

and $\Delta\alpha' = -\Delta\alpha$ replaces $\Delta\alpha$ for $\sum_{n=1}^{\frac{\sqrt{2}\pi}{\Delta\alpha}} \Delta\alpha = \sqrt{2}\pi$; $\sum_{n=1}^{\frac{\sqrt{2}\pi}{|\Delta\alpha'|}} |\Delta\alpha'| = \sqrt{2}\pi$

E Field:

$$\begin{bmatrix} x_2 \\ y_2 \\ z_2 \end{bmatrix} = \begin{bmatrix} \cos(\Delta\alpha) & -\sin^2(\Delta\alpha) & -\sin(\Delta\alpha)\cos(\Delta\alpha) \\ 0 & \cos(\Delta\alpha) & -\sin(\Delta\alpha) \\ \sin(\Delta\alpha) & \cos(\Delta\alpha)\sin(\Delta\alpha) & \cos^2(\Delta\alpha) \end{bmatrix} \begin{bmatrix} x_2' \\ y_2' \\ z_2' \end{bmatrix} \tag{117}$$

and $\Delta\alpha' = -\Delta\alpha$ replaces $\Delta\alpha$ for $\sum_{n=1}^{\frac{\sqrt{2}\pi}{\Delta\alpha}} \Delta\alpha = \sqrt{2}\pi$; $\sum_{n=1}^{\frac{\sqrt{2}\pi}{|\Delta\alpha'|}} |\Delta\alpha'| = \sqrt{2}\pi$

The field lines in the lab frame follow from the relativistic invariance of charge as given by Purcell [28]. The relationship between the relativistic velocity and the electric field of a moving charge shown schematically in Figure 9. From Eqs. (116-117) with $\sum_{n=1}^{\frac{\sqrt{2}\pi}{\Delta\alpha}} \Delta\alpha = \sqrt{2}\pi$, the photon equation in the lab frame of a right-handed circularly polarized photon orbitsphere is

$$\mathbf{E} = \mathbf{E}_0[\mathbf{x} + i\mathbf{y}]e^{-jkz}e^{-j\omega t} \tag{118}$$

$$\mathbf{H} = \left(\frac{\mathbf{E}_0}{\eta}\right)[\mathbf{y} - i\mathbf{x}]e^{-jkz}e^{-j\omega t} = \mathbf{E}_0\sqrt{\frac{\varepsilon}{\mu}}[\mathbf{y} - i\mathbf{x}]e^{-jkz}e^{-j\omega t} \tag{119}$$

with a wavelength of

$$\lambda = 2\pi\frac{c}{\omega} \tag{120}$$

The relationship between the photon orbitsphere radius and wavelength is

$$2\pi r_0 = \lambda_0 \tag{121}$$

The electric field lines of a right-handed circularly polarized photon orbitsphere as seen along the axis of propagation in the lab inertial reference frame as it passes a fixed point is shown in Figure 10.

Spherical Wave

Photons superimpose, and the amplitude due to N photons is

$$\mathbf{E}_{total} = \sum_{n=1}^{N} \frac{e^{-ik|\mathbf{r}-\mathbf{r}'|}}{4\pi|\mathbf{r}-\mathbf{r}'|} f(\theta,\phi) \tag{122}$$

In the far field, the emitted wave is a spherical wave

$$\mathbf{E}_{total} = E_o \frac{e^{-ikr}}{r} \tag{123}$$

The Green Function is given as the solution of the wave equation. Thus, the superposition of photons gives the classical result. As r goes to infinity, the spherical wave becomes a plane wave. The double slit interference pattern is predicted. From the equation of a photon, the wave-particle duality arises naturally. The energy is always given by Planck's equation; yet, an interference pattern is observed when photons add over time or space.

EQUATIONS OF THE FREE ELECTRON

Charge Density Function

The radius of an electron orbitsphere increases with the absorption of electromagnetic energy [29]. With the absorption of a photon of energy exactly equal to the ionization energy, the electron becomes ionized and is a plane wave (spherical wave in the limit) with the de Broglie wavelength. The ionized electron traveling at constant velocity is nonradiative and is a two dimensional surface having a total charge of e and a total mass of m_e. The solution of the boundary value problem of the free electron is given by the projection of the orbitsphere into a plane that linearly propagates along an axis perpendicular to the plane where the velocity of the plane and the orbitsphere is given by

$$v = \frac{\hbar}{m_e \rho_0} \tag{124}$$

and the radius of the orbitsphere in spherical coordinates is equal to the radius of the free electron in cylindrical coordinates ($\rho_0 = r_0$). The mass density function of a free electron shown in Figure 11 is a two dimensional disk having the mass density distribution in the xy(ρ)-plane

$$\rho_m(\rho,\phi,z) = \frac{m_e}{\frac{2}{3}\pi\rho_0^{\,3}} \pi\left(\frac{\rho}{2\rho_o}\right)\sqrt{\rho_0^{\,2}-\rho^2}\,\delta(z) \tag{125}$$

and charge-density distribution, $\rho_e(\rho,\phi,z)$, in the xy-plane given by replacing m_e with e. The charge density distribution of the free electron has recently been confirmed experimentally [30-31]. Researchers working at the Japanese National Laboratory for High Energy Physics (KEK) demonstrated that the charge of the free electron increases toward the particle's core and is symmetrical as a function of ϕ. In addition, the wave-particle duality arises naturally, and the result is consistent with scattering experiments from helium and the double split experiment [6].

Current Density Function

Consider an electron initially bound as an orbitsphere of radius $r = r_n = r_o$ ionized from a hydrogen atom with the magnitude of the angular velocity of the orbitsphere is given by

$$\omega = \frac{\hbar}{m_e r^2} \tag{126}$$

The current-density function of the free electron propagating with velocity v_z along the z-axis in the inertial frame of the proton is given by the vector projection of the current into xy-plane as the radius increases from $r = r_o$ to $r = \infty$. The current-density function of the free electron, is

$$\mathbf{J}(\rho,\phi,z,t) = \left[\pi\left(\frac{\rho}{2\rho_o}\right) \frac{e}{\frac{4}{3}\pi\rho_0^{\,3}} \frac{\hbar}{m_e\sqrt{\rho_0^{\,2}-\rho^2}}\, \mathbf{i}_\phi \right] \tag{127}$$

where $\rho_o = r_o$. The angular momentum, $\mathbf{L}$, is given by

$$\mathbf{L}\mathbf{i}_z = m_e r^2 \omega \tag{128}$$

Substitution of m_e for e in Eq. (127) followed by substitution into Eq. (128) gives the angular momentum density function, $\mathbf{L}$

$$\mathbf{L}\mathbf{i}_z = \pi\left(\frac{\rho}{2\rho_o}\right) \frac{m_e}{\frac{4}{3}\pi\rho_0^{\,3}} \frac{\hbar}{m_e\sqrt{\rho_0^{\,2}-\rho^2}} \rho^2 \tag{129}$$

The total angular momentum of the free electron is given by integration over the two dimensional disk having the angular momentum density given by Eq. (129).

$$\mathbf{L}\mathbf{i}_z = \int_0^{2\pi}\int_0^{\rho_0} \pi\left(\frac{\rho}{2\rho_o}\right) \frac{m_e}{\frac{4}{3}\pi\rho_0^{\,3}} \frac{\hbar}{m_e\sqrt{\rho_0^{\,2}-\rho^2}} \rho^2 \rho d\rho d\phi = \hbar \tag{130}$$

The four dimensional spacetime current-density function of the free electron that propagates along the z-axis with velocity given by Eq. (124) corresponding to $r = r_o = \rho_0$ is given by substitution of Eq. (124) into Eq. (128).

$$\mathbf{J}(\rho,\phi,z,t)=\left[\pi\left(\frac{\rho}{2\rho_o}\right)\frac{e}{\frac{4}{3}\pi\rho_0^{\,3}}\frac{\hbar}{m_e\sqrt{\rho_0^{\,2}-\rho^2}}\,\mathbf{i}_\varphi\right]+\frac{e\hbar}{m_e\rho_0}\delta(z-\frac{\hbar}{m_e\rho_0}t)\mathbf{i}_z \tag{131}$$

The spacetime Fourier Transform of is

$$\frac{e}{\frac{4}{3}\pi\rho_0^{\,3}}\frac{\hbar}{m_e}\mathrm{sinc}(2\pi s\rho_o)+2\pi e\frac{\hbar}{m_e\rho_0}\delta(\omega-\mathbf{k}_z\bullet\mathbf{v}_z) \tag{132}$$

The boundary condition is—spacetime harmonics of $\frac{\omega_n}{c}=k$ *or* $\frac{\omega_n}{c}\sqrt{\frac{\varepsilon}{\varepsilon_o}}=k$ do not exist. Radiation due to charge motion does not occur in any medium when this boundary condition is met. Thus, no Fourier components that are synchronous with light velocity with the propagation constant $|\mathbf{k}_z|=\frac{\omega}{c}$ exist, and radiation due to charge motion of the free electron does not occur when this boundary condition is met. It follows from Eq. (124) and the relationship $2\pi\rho_o=\lambda_o$ that the wavelength of the free electron is the de Broglie wavelength.

$$\lambda_o=\frac{h}{m_e v_z}=2\pi\rho_o \tag{133}$$

In the presence of a z-axis-applied magnetic field, the free electron precesses. The time average vector projection of the total angular momentum of the fee electron onto an axis S that rotates about the z-axis is $\pm\sqrt{\frac{3}{4}}\hbar$, and the time averaged projection of the angular momentum onto the axis of the applied magnetic field is $\pm\frac{\hbar}{2}$. Magnetic flux is linked by the electron in units of the magnetic flux quantum with conservation of angular momentum as in the case of the orbitsphere as the projection of the angular momentum along the magnetic field axis of $\frac{\hbar}{2}$ reverses direction. The energy, ΔE_{mag}^{spin}, of the spin flip transition corresponding to the $m_S=\frac{1}{2}$ quantum number is given by Eq. (64).

$$\Delta E_{mag}^{spin}=g\mu_B B \tag{134}$$

The Stern-Gerlach experiment implies a magnetic moment of one Bohr magneton and an associated angular momentum quantum number of 1/2. Historically, this quantum number is called the spin quantum number, m_S, and that designation is maintained.

TWO ELECTRON ATOMS

Two electron atoms may be solved from a central force balance equation with the nonradiation condition. The force balance equation is

$$\frac{m_e}{4\pi r_2^2}\frac{v_2^2}{r_2} = \frac{e}{4\pi r_2^2}\frac{(Z-1)e}{4\pi\varepsilon_o r_2^2} + \frac{1}{4\pi r_2^2}\frac{\hbar^2}{Zm_e r_2^3}\sqrt{s(s+1)} \tag{135}$$

which gives the radius of both electrons as

$$r_2 = r_1 = a_0\left\{\frac{1}{Z-1} - \frac{\sqrt{s(s+1)}}{Z(Z-1)}\right\};\ s = \frac{1}{2} \tag{136}$$

Ionization Energies Calculated using the Poynting Power Theorem

For helium, which has no electric field beyond r_1

$$Ionization\ Energy(He) = -E(electric) + E(magnetic) \tag{137}$$

where,

$$E(electric) = -\frac{(Z-1)e^2}{8\pi\varepsilon_o r_1} \tag{138}$$

$$E(magnetic) = \frac{2\pi\mu_0 e^2\hbar^2}{m_e^2 r_1^3} \tag{139}$$

For $3 \le Z$

$$Ionization\ Energy = -Electric\ Energy - \frac{1}{Z}Magnetic\ Energy \tag{140}$$

The energies of several two-electron atoms are given in Table 1.

ELASTIC ELECTRON SCATTERING FROM HELIUM ATOMS

The aperture distribution function, $a(\rho,\phi,z)$, for the elastic scattering of an incident electron plane wave represented by $\pi(z)$ by a helium atom represented by

$$\frac{2}{4\pi(0.567a_o)^2}[\delta(r-0.567a_o)] \tag{141}$$

is given by the convolution of the plane wave with the helium atom function:

$$a(\rho,\phi,z) = \pi(z)\otimes\frac{2}{4\pi(0.567a_o)^2}[\delta(r-0.567a_o)] \tag{142}$$

The aperture function is

$$a(\rho,\phi,z) = \frac{2}{4\pi(0.567a_o)^2}\sqrt{(0.567a_o)^2 - z^2}\,\delta(r-\sqrt{(0.567a_o)^2 - z^2}) \tag{143}$$

Far Field Scattering (circular symmetry)

Applying Huygens' principle to a disturbance caused by the plane wave electron over the helium atom as an aperture gives the amplitude of the far field or Fraunhofer diffraction pattern $F(s)$ as the Fourier Transform of the aperture distribution. The intensity I_1^{ed} is the square of the amplitude.

$$F(s) = \frac{2}{4\pi(0.567a_o)^2} 2\pi \int_0^{\infty} \int_{-\infty}^{\infty} \sqrt{(0.567a_o)^2 - z^2}\,\delta(\rho - \sqrt{(0.567a_o)^2 - z^2})\,J_o(s\rho)e^{-i(wz)}\rho d\rho dz \qquad (144)$$

$$I_1^{ed} = F(s)^2$$

$$= I_e \left\{ \left[\frac{2\pi}{(z_o w)^2 + (z_o s)^2} \right]^{\frac{1}{2}} \left\{ 2\left[\frac{z_o s}{(z_o w)^2 + (z_o s)^2} \right] J_{3/2}\left[((z_o w)^2 + (z_o s)^2)^{1/2} \right] - \left[\frac{z_o s}{(z_o w)^2 + (z_o s)^2} \right]^2 J_{5/2}\left[((z_o w)^2 + (z_o s)^2)^{1/2} \right] \right\} \right\}^2 \qquad (145)$$

$$s = \frac{4\pi}{\lambda} \sin\frac{\theta}{2};\ w = 0\ (units\ of\ \mathring{A}^{-1}) \qquad (146)$$

The experimental results of Bromberg [34], the extrapolated experimental data of Hughes [34], the small angle data of Geiger [35] and the semiexperimental results of Lassettre [34] for the elastic differential cross section for the elastic scattering of electrons by helium atoms is shown graphically in Figure 12. The elastic differential cross section as a function of angle numerically calculated by Khare [34] using the first Born approximation and first-order exchange approximation also appear in Figure 12. These results which are based on a quantum mechanical model are compared with experimentation [34-35]. The closed form function (Eqs. (145) and (146)) for the elastic differential cross section for the elastic scattering of electrons by helium atoms is shown graphically in Figure 13. The scattering amplitude function, $F(s)$ (Eq. (144), is shown as an insert. It is apparent from Figure 12 that the quantum mechanical calculations fail completely at predicting the experimental results at small scattering angles; whereas, there is good agreement between Eq. (145) and the experimental results.

THEORY OF FREE ELECTRON BUBBLES IN SUPERFLUID HELIUM

Recently a new challenge to the fundamental foundations of quantum mechanics has arisen based on experiments of free electrons injected into superfluid helium. In order to explain the increase in conductivity observed when electrons in superfluid helium are irradiated with light, British physicist Humphrey Maris has proposed [2] that the electron breaks into equal sized fragments which he calls "electrinos". According to Maris, this process of division of the electron may continue to such that the electron breaks into two and then the 1/2 electrons may divide into two forming 1/4 electrons, and the process may repeat indefinitely.

Electrons do not break into pieces. It is shown *infra* that the free electron in superfluid helium is an orbitsphere which can act as a resonator cavity and absorb resonant radiation to

form stable nonradiative states of radii $n = \frac{1}{\text{integer}}$ times that of the radius of the electron without an absorbed photon.

Stability of Fractional Principal Quantum States of Free Electrons in Liquid Helium

Photon absorption occurs as an excitation of a resonator mode; consequently, the hydrogen atomic energy states are quantized as a function of the parameter n as shown in the Excited States section. Each value of n in Eqs. (84-89) corresponds to an allowed transition caused by a resonant photon which excites the transition of the orbitsphere resonator cavity. In the case of free electrons in superfluid helium, the central field of the proton is absent; however, the electron is maintained as an orbitsphere by the pressure of the surrounding helium atoms. In this case, rather than the traditional integer values (1, 2, 3,...,) of n, values of fractions are allowed according to Eqs. (81-82) which correspond to transitions with an increase in the effective central field and a decrease in the radius of the orbitsphere. In these cases, the electron undergoes a transition to a stable higher energy state. The trapped photon electric field which provides force balance for the orbitsphere is a solution of Laplace's equation in spherical coordinates is given by Eq. (84). The excited states of atomic hydrogen correspond to $n = 1,2,3,4,...$, and the free electron states in helium correspond to $n = \frac{1}{2},\frac{1}{3},\frac{1}{4},...,\frac{1}{p}$ where p is an integer. The implications to atomic hydrogen states was discussed previously [8].

In each case, the "trapped photon" is a "standing electromagnetic wave" which actually is a circulating wave that propagates around the z-axis, and its source current superimposes with each great circle current loop of the orbitsphere. The time-function factor, $k(t)$, for the "standing wave" is identical to the time-function factor of the orbitsphere in order to satisfy the boundary (phase) condition at the orbitsphere surface. Thus, the angular frequency of the "trapped photon" has to be identical to the angular frequency of the electron orbitsphere, ω_n, given by Eq. (9). Furthermore, the phase condition requires that the angular functions of the "trapped photon" have to be identical to the spherical harmonic angular functions of the electron orbitsphere. Combining $k(t)$ with the ϕ-function factor of the spherical harmonic gives $e^{i(m\phi-\omega_n t)}$ for both the electron and the "trapped photon" function. The angular functions in phase with the corresponding photon functions are given by Eqs. (14-15).

The solution of the "trapped photon" field of electrons in helium is analogous to those of hydrogen excited states except that $n = \frac{1}{\text{integer}}$ and the $-Y_0^0(\theta,\phi)$ term is not present since the central field of the proton is absent and the nature of the field at the origin is equivalent to the solution of the Poisson equation with a delta function inhomogeneity at the origin [36].

$$\mathbf{E}_{r\,photon\;n,l,m} = C\frac{e(na)^{\ell}}{4\pi\varepsilon_o}\frac{1}{r^{(\ell+2)}}\left[\frac{1}{n}\left[Y_0^0(\theta,\phi)+\mathrm{Re}\left\{Y_\ell^m(\theta,\phi)\left[1+e^{i\omega_n t}\right]\right\}\right]\right]\delta(r-r_n)$$

$$\omega_n = 0 \;\; for\; m = 0 \tag{147}$$

$$n = 1, \frac{1}{2}, \frac{1}{3}, \frac{1}{4}, \ldots, \frac{1}{p}$$

$$\ell = 1, 2, \ldots, n-1$$

$$m = -\ell, -\ell+1, \ldots, 0, \ldots, +\ell$$

In Eq. (147), a is the radius of the electron in helium without an absorbed photon. C is a constant expressed in terms of an equivalent central charge. It is determined by the force balance between the centrifugal force of the electron orbitsphere and the radial force provided by the pressure from the van der Waals force of attraction between helium atoms given *infra*.

For fractional quantum energy states of the electron, σ_{photon}, the two dimensional surface charge due to the "trapped photon" at the electron orbitsphere, follows from Eqs. (5.13) and (2.11) of Mills [6].

$$\sigma_{photon} = \frac{e}{4\pi(r_n)^2}\left[-\frac{1}{n}\left[Y_0^0(\theta,\phi)+\mathrm{Re}\left\{Y_\ell^m(\theta,\phi)\left[1+e^{i\omega_n t}\right]\right\}\right]\right]\delta(r-r_n) \quad n = 1, \frac{1}{2}, \frac{1}{3}, \frac{1}{4}, \ldots, \tag{148}$$

And, $\sigma_{electron}$, the two dimensional surface charge of the electron orbitsphere is

$$\sigma_{electron} = \frac{-e}{4\pi(r_n)^2}\left[Y_0^0(\theta,\phi)+\mathrm{Re}\left\{Y_\ell^m(\theta,\phi)\left[1+e^{i\omega_n t}\right]\right\}\right]\delta(r-r_n) \tag{149}$$

The superposition of σ_{photon} (Eq. (148)) and $\sigma_{electron}$, (Eq. (149)) where the spherical harmonic functions satisfy the conditions given in the Angular Function section [6] is a radial electric monopole represented by a delta function.

$$\sigma_{photon} + \sigma_{electron} = \frac{-e}{4\pi(r_n)^2}\frac{1}{n}\left[Y_0^0(\theta,\phi)+\mathrm{Re}\,Y_\ell^m(\theta,\phi)\left[1+e^{i\omega_n t}\right]\right]\delta(r-r_n) \quad n = 1, \frac{1}{2}, \frac{1}{3}, \frac{1}{4}, \ldots, \tag{150}$$

As given in the Nonradiation Based on Haus' Condition section, the radial delta function does not possess spacetime Fourier components synchronous with waves traveling at the speed of light (Eqs. (16)). Thus, the fractional quantum energy states are stable.

The speed of light in vacuum c is given by

$$c = \frac{1}{\sqrt{\mu_0\varepsilon_0}} \tag{151}$$

where μ_o is the permeability of free-space and ε_o is the permittivity of free-space. The wavenumber is given by

$$k_{vacuum} = \frac{2\pi}{\lambda} = \omega\sqrt{\mu_0\varepsilon_0} \tag{152}$$

The speed of light in a medium such as superfluid helium v is given by

$$v = \frac{1}{\sqrt{\mu_0 \varepsilon}} \tag{153}$$

where μ_o is the permeability of free-space and ε is the permittivity of the medium. The wavenumber is given by

$$k_{medium} = \frac{2\pi}{\lambda} = \omega\sqrt{\mu_0 \varepsilon} \tag{154}$$

The ratio of the wavenumber in vacuum and the wavenumber in superfluid helium is given by

$$\frac{k_{helium}}{k_{vacuum}} = \frac{\frac{2\pi}{\lambda_{helium}}}{\frac{2\pi}{\lambda_{vacuum}}} = \frac{\omega\sqrt{\mu_0 \varepsilon}}{\omega\sqrt{\mu_0 \varepsilon_0}} \tag{155}$$

The frequency of the photon in free space and in helium at the electron must be the same. Thus,

$$k_{helium} = k_{vacuum}\frac{\varepsilon}{\varepsilon_0} \tag{156}$$

Since $\varepsilon > \varepsilon_0$, the wavenumber in helium is greater than the wavenumber in vacuum. Thus, a photon traveling in liquid helium may excite a mode in an electron bubble which is nonradiative. In this case, spacetime harmonics of $\frac{\omega_n}{c} = k$ or $\frac{\omega_n}{c}\sqrt{\frac{\varepsilon}{\varepsilon_o}} = k$ for which the Fourier transform of the current-density function is nonzero do not exist. Radiation due to charge motion does not occur in any medium when this boundary condition is met.

As discussed *infra.*, the phenomenon of photon absorption by electrons in superfluid helium to give rise to an increase in conductivity is temperature dependent. This temperature dependence may be explained on the basis of the loss of viscosity of superfluid helium that is permissive of an electron supercurrent. That is, at 1.7 K, the viscosity is sufficiently close to zero such that the angular current of the electron may propagate without energy loss. Roton scattering dominates over phonon scattering at this temperature and below [37]. Then, the two dimensional surface charge due to a "trapped photon" at the electron orbitsphere of a free electron in helium is given by Eq. (150) such that the corresponding state is stable. Resonant photon absorption may occur between these stable states. The central force which results in a fractional electron radius compared to the unexcited electron is provided by the absorbed photon as discussed in the Superfluid Helium Ion Mobility Results and Discussion section.

SUPERFLUID HELIUM ION MOBILITY RESULTS AND DISCUSSION

Experiments to study the effect of light on ion mobility have been conducted by Northby and Sanders [38-39], Zipfel and Sanders [40-41], and Grimes and Adams [42-43]. For example, in the Northby and Sanders experiments [38-39], ions were introduced into the liquid

from a radioactive source, and had to pass through two grids in order to reach the detector. The voltages on the grids were varied in time in a way such that normal negative ions could not reach the detector. It was found that when the liquid was illuminated, a small ion current reached the detector. Thus, they observed an increase in ion mobility under illumination, but recognized that the origin of the effect was unclear. It appears that the absorption of a photon by an electron bubble or orbitsphere in superfluid helium provides a natural explanation for the majority of the photo-conductivity results.

The photon absorption is determined by the correspondence principle—the conservation of the $\hbar$ of angular momentum of the free space photon and the equivalent change in the angular momentum of the electron upon excitation. Thus, the radius of the electron following the absorption of a resonant photon is given by $n = \frac{1}{\text{integer}}$ times that of the original radius.

$$r = nr_1 \tag{157}$$

where $n = \frac{1}{\text{integer}}$ and r_1 is the radius of the electron in superfluid helium which has not absorbed a photon. This radius is determined by a force balance between the van der Waals pressure (force per unit area) of superfluid helium and the centrifugal force of the electron. The latter is given by

$$\mathbf{F}_{centrifugal} = \frac{m_e}{4\pi r_1^2}\frac{\mathbf{v}_1^2}{r_1} \tag{158}$$

where $\frac{m_e}{4\pi r_1^2}$ is the mass density of the orbitsphere and $\mathbf{v}_1$ is given by Eq. (6). The radius r_1 can be determined from the photo-conductivity experiments of Zipfel and Sanders [41]. At zero pressure a photo-conductivity peak was observed at approximately $0.5\,eV$. From Eqs. (87-89), the change in the frequency of the electron which matches frequency of the exciting photon is given by

$$\omega_{photon} = \frac{\hbar}{m_e r_1^2}\left[\frac{1}{n^2} - 1\right] \tag{159}$$

where $n = \frac{1}{\text{integer}}$. The radius r_1 is given by

$$r_1 = \sqrt{\frac{\hbar}{m_e \omega_{photon}}\left(\frac{1}{n^2} - 1\right)} \tag{160}$$

The relationship between energy and angular frequency of a photon is given by Planck's equation.

$$E = \hbar\omega_{photon} \tag{161}$$

The angular frequency corresponding to a photon of $0.5\,eV$ is

$$\omega_{photon} = \frac{8.0 X 10^{-20}\ J}{\hbar} = 7.6\ X 10^{14}\ rad/\sec \tag{162}$$

In the case that $0.5\ eV$ is the lowest energy transition for an electron in superfluid helium, the $n = 1 \rightarrow n = \frac{1}{2}$ transition corresponds to $n = \frac{1}{2}$ in Eq. (159). From Eq. (159) and Eq. (162), the radius r_1 is

$$r_1 = \sqrt{\frac{\hbar}{m_e\left(7.6\ X 10^{14}\ rad/\sec\right)}\left(\frac{1}{\left(\frac{1}{2}\right)^2} - 1\right)} = 6.7\ X 10^{-10}\ m = 6.7\ \text{Å} \tag{163}$$

where $n = \frac{1}{2}$. Comparing the case of the electron of a hydrogen atom to the case of an electron in helium, no initial central Coulomb field due to a proton is present, and the electron increases in kinetic energy upon photon absorption. Thus, the energy required to cause a transition in the latter case is twice that of the former. The photon stores energy in the electric field of the resonator mode and increases the potential energy of the electron. The potential is the sum of the binding energy and the kinetic energy. The corresponding photon wavelength that will be absorbed by the electron is $2.5\ \mu m$.

The radius calculated in Eq. (163), is an approximation since the energy due to the pressure volume work and the surface energy change of the bubble were neglected. The former is given by

$$P\int dV = \frac{4}{3}\pi\left(r_1^3 - r_n^3\right)P \tag{164}$$

where P is the applied pressure, the integral is over the volume of the bubble, and r_1 and r_n are the initial and final radii of the electron bubble. The latter is given by

$$\alpha\int dA = 4\pi\left(r_1^2 - r_n^2\right)\alpha \tag{165}$$

where α is the surface energy of helium per unit area, the integral is over the surface of the bubble, and r_1 and r_n are the initial and final radii of the electron bubble.

The contribution of these terms can be estimated by comparing the next experimental photo-conductivity peak at higher energy compared to the prediction given by Eqs. (159) and (161). Northby and Sanders [38-39] found that in the range of $0.7\ eV$ to $3\ eV$ the photo-induced current had a peak when the photon energy was $1.21\ eV$ at zero pressure. Zipfel and Sanders [40-41] confirmed the peak at $1.21\ eV$. In experiments similar to those of Northby and Sanders [38-39], Zipfel and Sanders [40-41] made measurements of the photo-conductivity as a function of pressure up to 16 bars. The photo-conductivity peak detected by Northby and Sanders [38-39] was found to shift to higher photon energies as the pressure increased. This is expected since the radius of the normal electron decreases and the corresponding initial

angular frequency increases with increasing pressure. Thus, the transition angular frequencies and energies increase (Eq. (159).

The next higher energy transition for an electron in superfluid helium is $n = 1 \rightarrow n = \frac{1}{3}$. The transition energy corresponds to $n = \frac{1}{3}$ in Eqs. (159) and (161). The calculated energy neglecting the energy due to the pressure volume work and the surface energy change of the bubble is

$$E = \hbar\omega_{photon} = \frac{\hbar^2}{m_e r_1^2}\left[\frac{1}{\left(\frac{1}{3}\right)^2} - 1\right] = \frac{\hbar^2}{m_e\left(6.7\ X\ 10^{-10}\ m\right)^2}\left[\frac{1}{\left(\frac{1}{3}\right)^2} - 1\right] = 1.3\ eV \qquad (166)$$

where r_1 is given by Eq. (163). Given the experimental uncertainty of the energy of the lowest energy transition, 1.21 eV, this result confirms that the contributions due to pressure volume work and the surface energy change of the bubble may be neglected.

In the experiments of Northby and Sanders [38-39], Zipfel and Sanders [40-41], and Grimes and Adams [42-43], it was noted that the photo-conductivity effect was absent above a critical temperature. This temperature was approximately 1.7 K at zero pressure, and decreased to 1.2 K at 20 bars. Roton scattering dominates over phonon scattering at 1.7 K and below [37]. The photo-conductivity signal disappears because of phonon excitation of the bubble motion which causes the excited electron state to decay. As the pressure is increased, the roton energy gap goes down, and so the phonon scattering increases. Thus, it is to be expected that the critical temperature decreases with increasing pressure.

Each stable excited state electron bubble which has a radius of $\frac{r_1}{\text{integer}}$ may migrate in an applied electric field. The bubble may be scattered by rotons, phonons, and He^3 impurities. At temperatures less that 1.7 K, roton scattering dominates [37]. An equation for the electron bubble mobility is derived by Baym, Barrera, and Pethick [44] in terms of the roton-bubble momentum transfer cross section by calculating the rate of roton-bubble momentum transfer using a statistical mechanical approach. In the case of an elementary excitation $\vec{k}$ scattered by the bubble with a differential cross section $\sigma(k,\theta)$ and obeying $|\vec{k}'| \cong |\vec{k}|$, their result may be written

$$\frac{e}{\mu} = -\frac{\hbar^2}{6\pi^2}\int_0^\infty k^4 \frac{\delta n}{\delta\varepsilon} v_g(k)\sigma_T(k)dk \qquad (167)$$

where μ is the bubble mobility, n is the distribution function of the excitation, $v_g(k)$ is the group velocity of the excitation, and $\sigma_T(k)$ is the momentum-transfer cross section defined by

$$\sigma_T(k) = \int (1 - \cos\theta)\sigma(k,\theta)d\Omega \qquad (168)$$

Schwarz and Stark [37] made the reasonable assumption that $\sigma_T(k)$ is a weak function of $k-k_0$. Because of the strong minimum at $k_0 = 1.91$ Å^{-1} in the roton energy spectrum, Eq. (167) then gives to a good approximation

$$\mu = \frac{3\pi^2 e}{\hbar k_0^4 \sigma_T(k_0)} \exp(\Delta / k_B T) = \frac{3.38\ X\ 10^{-25}\ m^4 V^{-1} \sec^{-1}}{\sigma_T(k_0)} \exp(8.65\ K/T) \tag{169}$$

where $\Delta / k_B = 8.65 \pm 0.04\ K$ is the roton energy gap derived from neutron scattering [45]. Schwarz and Stark [37] propose that the roton de Broglie wavelength corresponding to $k_0 = 1.91$ Å^{-1} is $\lambda_0 = 3.3$ which is small compared with $\sqrt{\frac{\sigma_T(k_0)}{\pi}}$; thus, the collision cross section may be nearly geometrical. Although the roton carries a great deal of energy and momentum, its effective mass is much less than that of the ion. Assume that the scattering is elastic, then $|\vec{k}'| \cong |\vec{k}|$ is satisfied. They conclude a hard-sphere cross section given by

$$\sigma_T(k_0) \cong \pi(a_+ + a_r)^2 \tag{170}$$

where a_+ is the radius of the ion and a_r is the effective collision radius of the roton. Using experimental values for a_+ and $\sigma_T(k)$, they find that

$$a_r = 3.7 \pm 0.2\ \text{Å} \tag{171}$$

They surmise from this that the roton is localized within a region of radius $\approx 3.7 - 4.0$ Å, and that it interacts strongly with any disturbance which penetrates this region. They point out that $\approx 3.7 - 4.0$ Å is only slightly larger than the nearest neighbor distance in liquid helium [46] and that a roton may thus be pictured as a highly correlated motion of an energetic He^4 atom and its nearest neighbors only.

The geometric cross-section of the normal electron bubble σ_e is given as

$$\sigma_e = \pi r_1^2 \tag{172}$$

where r_1 is the radius of the unexcited electron bubble given by Eq. (163). From Eq. (163) and Eqs. (169-172), the mobility of the normal electron bubble is given by

$$\mu = \frac{3\pi^2 e}{\hbar k_0^4 \pi (a_r + r_1)^2} \exp(\Delta / k_B T) = \frac{3.38\ X\ 10^{-25}\ m^4 V^{-1} \sec^{-1}}{\pi (3.7\ X\ 10^{-10}\ m + 6.7\ X\ 10^{-10}\ m)^2} \exp(8.65\ K/T) \tag{173}$$

At $1\ K$, Eq. (173) gives $\mu = 5.7\ cm^2 V^{-1} \sec^{-1}$ for the mobility of the normal electron bubble ($n = 1$) which is in reasonable agreement with the experimental value of $5\ cm^2 V^{-1} \sec^{-1}$ from Figure 14.

The normal electron bubble has a uniform constant spherical charge density. This charge density may be modulated by a time and spherically harmonic function as given by Eq. (15). In the case of excited state electron bubbles, the contribution to the roton scattering cross section given by Eq. (168) is larger than the geometric cross section given in Eq. (172) where the radius is given by Eq. (157). In this case, $\sigma_T(k)$ given by Eq. (168) follows the derivation

of Baym, Barrera, and Pethick [47] where the spherical harmonic angular function causes a gain in the scattering cross section that may be modeled after that of a Hertzian dipole antenna. The radiation power pattern of a Hertzian dipole is given by Kong [48]. The radiation power pattern is

$$\langle \mathrm{S} \rangle = \frac{1}{2}\mathrm{Re}[\mathbf{E} \times \mathbf{H}] = \hat{\mathbf{r}}\frac{\eta}{2}\left(\frac{k|I|\Delta z}{4\pi r}\right)\sin^2\theta \tag{174}$$

where I is the current, Δz is the length of the dipole, and η is the impedance of free space. The antenna directive gain $D(\theta,\varphi)$ is defined as the radiation of the Poynting power density $\langle S_r \rangle$ over the power P, divided by the area of the sphere:

$$D(\theta,\phi) = \frac{\langle S_r \rangle}{P/4\pi r^2} = \frac{3}{2}\sin^2\theta \tag{175}$$

The plot of $D(\theta,\varphi)$ given by Eq. (175) is known as the gain pattern. The directivity of an antenna is defined as the value of the gain in the direction of its maximum value. For the Hertzian dipole the maximum of 1.5 occurs at $\theta = \frac{\pi}{2}$. Thus, the directivity of a Hertzian dipole is 1.5.

The spherical harmonic angular functions are

$$Y_{lm}(\theta,\phi) = \sqrt{\frac{(2l+1)(l-m)!}{4\pi(l+m)!}}P_l^m(\cos\theta)e^{im\phi} = N_{\ell,m_\ell}P_l^m(\cos\theta)e^{im\phi} \tag{176}$$

where is the normalization constant given by

$$N_{\ell,m_\ell} = \sqrt{\frac{(2l+1)(l-m)!}{4\pi(l+m)!}} \tag{177}$$

In the case of excited states, $\sigma(k,\theta)$ of Eq. (168) is

$$\sigma(k,\theta) = k^{-2}\left|\frac{\int P_0^0(\cos\theta)e^{i0\phi}d\Omega}{\int P_l^m(\cos\theta)e^{im\phi}d\Omega}\right|^2 = k^{-2}\left(\frac{N_{\ell,m_\ell}}{N_{0,0}}\right)^2 \tag{178}$$

For excited states, the geometric cross-section of the electron bubble σ_e is then given as

$$\sigma_e = \pi n r_{n,\ell,m_\ell}^2 \tag{179}$$

where

$$r_{n,\ell,m_\ell} = \frac{N_{\ell,m_\ell}}{N_{0,0}}nr_1 \tag{180}$$

r_1 is the radius of the unexcited electron bubble given by Eq. (163) and $n = \frac{1}{\text{integer}}$. The angular parameters $\frac{N_{\ell,m_\ell}}{N_{0,0}}$ are given with the first few spherical harmonics in Table 2. In this case, $\sigma_T(k)$ is given by Eq. (168) where r_1 is replaced by r_{n,ℓ,m_ℓ} (Eq. (180)). The roton scattering cross section given by the hard-sphere cross section is then

$$\sigma_T(k_0) \cong \pi\left(r_{n,\ell,m_\ell} + a_r\right)^2 \tag{181}$$

where a_r is the effective collision radius of the roton given by Eq. (171). From Eq. (173) and Eqs. (180-181), the mobilities of electron bubbles are given by

$$\mu = \frac{3\pi^2 e}{\hbar k_0^4 \pi\left(a_r + r_{n,\ell,m_\ell}\right)^2} \exp\left(\Delta / k_B T\right) = \frac{3.38\ X\ 10^{-25}\ m^4 V^{-1} \sec^{-1}}{\pi\left(3.7\ X\ 10^{-10}\ m + n\frac{N_{\ell,m_\ell}}{N_{0,0}} 6.7\ X\ 10^{-10}\ m\right)^2} \exp(8.65\ K/T) \tag{182}$$

where $n = \frac{1}{\text{integer}}$. The mobility of an excited state electron bubble having a fractional principal quantum number ($n = \frac{1}{\text{integer}}$) relative to the normal electron bubble as a function of quantum numbers n, ℓ, and m_ℓ is given in Table 3. A plot of Eq. (182) normalized to the mobility of the normal bubble as a function of p corresponding to fractional principal quantum number $n = \frac{1}{\text{integer}} = 1/p$ for given ℓ, and m_ℓ quantum numbers appears in Figure 15.

Using time-of-flight, Doake and Gribbon [49] detected negatively-charged ions that had a mobility substantially higher than the normal electron bubble negative ion. This ion, which has become known as the "fast ion", was next seen in another time-of-flight experiment by Ihas and Sanders in 1971 [50]. They showed that the fast ion could be produced by an α or β source, or by an electrical discharge in the helium vapor above the liquid. In addition, they reported the existence of two additional negative carriers, referred to as "exotic ions", that had mobilities larger than the mobility of the normal negative ion, but less than the mobility of the fast ion. These exotic ions were detected only when there was an electrical discharge above the liquid surface. In a paper the following year [51], Ihas and Sanders (IS) reported on further experiments in which at least 13 carriers with different mobilities were detected. The experimental details are described in the thesis of Ihas [52]. Eden and McClintock (EM) [53-54] also detected as many as 13 ions with different mobilities. Both IS and EM put forward a number of proposals to explain the exotic ions, but all of these proposals were shown to be unsatisfactory by Maris [2]. It is significant that the exotic ions appear only when an electrical discharge takes place close to the free surface of the liquid. Under these conditions, the electrons that enter the liquid and form bubbles may absorb light emitted from the discharge. Thus, it is natural to consider the possibility that the exotic ions are electron bubbles in fractional energy states.

The mobility of several electron bubbles in superfluid helium plotted versus the inverse of the temperature is shown in Figure 14. The temperature dependence of the mobility predicted by Eq. (182) is in good agreement with the data of Ihas [52] and the plots of Maris

[2]. The ion assignments given in Figure 14 are based on their mobilities relative to the normal ion as given in Table 4.

Following a pulse discharge with an electric field applied to superfluid helium, Ihas [52] recorded ion peaks using time of flight. Fifteen ion peaks recorded by Ihas and Sanders are identified in Figure 16. The mobilities relative to the normal electron bubble ($n = 1$) are given in Table 4. The assignments of the mobilities of excited state electron bubbles having fraction principal quantum number ($n = \frac{1}{\text{integer}}$) relative to the normal electron bubble as a function of quantum numbers n, ℓ, and m_ℓ is also given in Table 4 based on the theoretical valves given in Table 3. The agreement between theory and experiment is excellent.

Peaks 14-15 of Figure 16 and Table 4 represent a band with a cutoff at a migration velocity of about 7.5 times the velocity of the normal ion as $n = \frac{1}{\text{integer}}$ approaches zero ($n = \frac{1}{100}$ was used to calculate this limiting case). The electron radius is predicted to decrease such that the effective collision radius of the roton determines the maximum mobility as given by Eq. (182). The theoretically predicted maximum of electron bubble mobility of about seven times that of the normal ion is confirmed by the Ihas data [52] where the band comprising peaks 14-15 correspond to $n \leq \frac{1}{7}$. Furthermore, Eden and McClintock [53] and Doake and Gribbon [49] measured the drift velocity as a function of applied electric field. The fast ion showed a slope of the drift velocity versus applied electric field of about seven times that of the normal ion. Thus, these results agree with the data of Ihas and with theoretical predictions.

The small deviation of the data from the theoretical in Table 4 may be due to differences in ion production rates and mechanisms based on the spectrum of the arc. Transitions between states may also be a peak broadened factor wherein a peak undergoes a transition to a faster or slower state during migration. This may provide an explanation for the large peak width of peak # 4 of Figure 16 as well as the broad continuum background in this region. Scattering other than roton scattering may also be involved, and these mechanisms such as phonon scattering and inter-bubble "impurity" scattering would effect larger ions more than smaller ions due to their larger geometric cross section. A preferred method to determine the migration times of each electron bubble ($n = \frac{1}{\text{integer}}$) is to cause the formation of each specific state with resonant radiation (Eq. (159) and Eq (161)) and to measure the migration time of each ion separately relative to the $n = 1$ bubble.

Using a time-of-flight method, Doake and Gribbon [49] discovered that a fast ion can exist in superfluid helium which unlike the normal ion may be accelerated to the Landau critical

velocity v_L for roton creation without undergoing metamorphosis to a charged vortex ring, even under the saturated vapor pressure. As a consequence, Eden and McClintock [53] studied the behavior of the exotic ions in strong electric field and reported evidence suggesting that intermediate mobility negative ions can nucleate quantized vortex rings in superfluid helium when subject to strong electric fields. Eden and McClintock observed that the drift velocity of intermediate ions may not be linear with electric field and that this effect varies with the particular intermediate ion. Eden and McClintock [53] further observed a decrease in drift velocities of intermediate ions with inter-ion variation for increasing sufficiently strong electric fields. They attributed this to the formation of negatively charged vortex rings. However, for an appropriate electric field, the drift velocity approaches a maximum independent of the field, and formation of charged vortex rings does not explain the field independence [53]. The limiting velocities shown in the data traces of Figure 17 may be a function of the size of the ion for all intermediate ions. In this case, the limiting velocity data of Eden and McClintock [53] are plotted in Figure 18 with the mobility of the normal ion as a function of p corresponding to principal quantum number $n = \frac{1}{\text{integer}} = 1/p$. The agreement between the experimental data and theoretical mobilities is excellent. The existence of multiple peaks under the fast peak such as peak #14 and #15 of Figure 16 is also supported by the data of Eden and McClintock [53] because the peak of highest mobility split into the two peaks shown in Figure 17 at higher fields.

CONCLUSION

Recently, the behavior of free electrons in superfluid helium has again forced the issue of the meaning of the wavefunction. Electrons form bubbles in superfluid helium which reveal that the electron is real and that a physical interpretation of the wavefunction is necessary. Furthermore, when irradiated with low energy light, the electrons carry increased current at different rates as if they exist with at least 15 different sizes. Peaks are observed in the photo-conductivity absorption spectrum at 0.5 and 1.21 eV. CQM [6] gives closed form physical solutions for the electron in atoms, the free electron, and the free electron in superfluid helium. The predicted photo-conductivity absorption spectrum and the mobilities of the 15 identified ions match the experimental results. The data support the existence of fractional principal quantum energy states of free electrons in superfluid helium. The results have implications that the concept of probability waves of quantum mechanics must be abandoned and atomic theory must be based in reality.

REFERENCES

1. F. Laloë, Do we really understand quantum mechanics? Strange correlations, paradoxes, and theorems, Am. J. Phys. 69 (6), June, (2001), pp. 655-701.
2. H. J. Maris, Journal of Low Temperature Physics, Vol. 120, (2000), p. 173.
3. P. Weiss, Science News, Vol. 158, No. 14, September 30, (2000), p. 216.
4. P. Ball, Nature, http://helix.nature.com/nsu/000921/000921-1.html.
5. I Jackson, New Scientist, October 14, (2000), http://www.newscientist.com/nl/1014/double.html.
6. R. Mills, *The Grand Unified Theory of Classical Quantum Mechanics*, January 2000 Edition, BlackLight Power, Inc., Cranbury, New Jersey, Distributed by Amazon.com; September 2001 Edition posted at www.blacklightpower.com.
7. R. Mills, "The Hydrogen Atom Revisited", Int. J. of Hydrogen Energy, **25**, Issue 12, December, (2000), pp. 1171-1183.
8. R. Mills, "The Nature of Free Electrons in Superfluid Helium--a Test of Quantum Mechanics and a Basis to Review its Foundations and Make a Comparison to Classical Theory", Int. J. Hydrogen Energy, Vol. 26, No. 10, (2001), pp. 1059-1096.
9. C. A. Fuchs, A. Peres, "Quantum Theory Needs No "Interpretation", Physics Today, March, (2000), p. 70.
10. S. Peil, G. Gabrielse, "Observing the Quantum Limit of an Electron Cyclotron: QND Measurements of Quantum Jumps between Fock States, Phys. Rev. Letts., Volume 83, No. 7, August 16, (1999), pp. 1287-1290.
11. Dyson, F., "Feynman's proof of Maxwell equations", Am. J. Phys., Vol. 58, (1990), pp. 209-211.
12. Horgan, J., "Quantum Philosophy", Scientific American, Vol. 267(1), July, (1992), p. 94.
13. H. A. Haus, On the radiation from point charges, American Journal of Physics, Vol. 54, (1986), pp. 1126–1129.
14. R. Mills, "The Grand Unified Theory of Classical Quantum Mechanics", Global Foundation Inc. Orbis Scientiae entitled *The Role of Attractive and Repulsive Gravitational Forces in Cosmic Acceleration of Particles The Origin of the Cosmic Gamma Ray Bursts*, (29th Conference on High Energy Physics and Cosmology Since 1964) Dr. Behram N. Kursunoglu, Chairman, December 14-17, 2000, Lago Mar Resort, Fort Lauderdale, FL, Kluwer Academic/Plenum Publishers, New York, pp. 243-258.
15. R. Mills, "The Grand Unified Theory of Classical Quantum Mechanics", Int. J. Hydrogen Energy, Vol. 27, No. 5, (2002), pp. 565-590.
16. McQuarrie, D. A., *Quantum Chemistry*, University Science Books, Mill Valley, CA, (1983), pp. 206-225.

17. L. C. Shi, J. A. Kong, *Applied Electromagnetism*, Brooks/Cole Engineering Division, Monterey, CA, (1983), pp. 170-209.
18. J. Daboul, J. H. D. Jensen, Z. Physik, Vol. 265, (1973), pp. 455-478.
19. J. D. Jackson, *Classical Electrodynamics*, Second Edition, John Wiley & Sons, New York, (1962), pp. 739-742.
20. D. A. McQuarrie, *Quantum Chemistry*, University Science Books, Mill Valley, CA, (1983), pp. 238-241.
21. R. S. Van Dyck, Jr., P. Schwinberg, H. Dehmelt, "New high precision comparison of electron and positron g factors", Phys. Rev. Lett., Vol. 21, (1987), p. 26-29.
22. T. A. Abbott, D. J. Griffiths, Am. J. Phys., Vol. 153, No. 12, (1985), pp. 1203-1211.
23. G. Goedecke, Phys. Rev., Vol. 135B, (1964), p. 281.
24. J. D. Jackson, *Classical Electrodynamics*, Second Edition, John Wiley & Sons, New York, (1962), pp. 739-779.
25. M. Mizushima, *Quantum Mechanics of Atomic Spectra and Atomic Structure*, W.A. Benjamin, Inc., New York, (1970), p.17.
26. J. D. Jackson, *Classical Electrodynamics*, Second Edition, John Wiley & Sons, New York, (1962), pp. 739-752.
27. J. D. Jackson, *Classical Electrodynamics*, Second Edition, John Wiley & Sons, New York, (1962), pp. 758-763.
28. E. Purcell, *Electricity and Magnetism*, McGraw-Hill, New York, (1965), pp. 156-167.
29. D. Clark, "Very large hydrogen atoms in interstellar space", Journal of Chemical Education, 68, No. 6, (1991), pp. 454-455.
30. J. Gribbin, New Scientist, January, 25, (1997), p. 15.
31. Levine, I., et al., Physical Review Letters, Vol. 78., No. 3, (1997), pp. 424-427.
32. C. E. Moore, "Ionization Potentials and Ionization Limits Derived from the Analyses of Optical Spectra, Nat. Stand. Ref. Data Ser.-Nat. Bur. Stand. (U.S.), No. 34, 1970.
33. R. C. Weast, *CRC Handbook of Chemistry and Physics*, 58 Edition, CRC Press, West Palm Beach, Florida, (1977), p. E-68.
34. P. J. Bromberg, Absolute differential cross sections of elastically scattered electrons. I. He, N2, and CO at 500 eV, *The Journal of Chemical Physics*, Vol. 50(9), (1969), pp. 3906-3921.
35. J. Geiger, Elastische und unelastische streuung von elektronen an gasen, *Zeitschrift fur Physik*, Vol. 175, (1963), pp. 530-542.
36. Jackson, J. D., *Classical Electrodynamics*, Second Edition, John Wiley & Sons, New York, (1962), pp. 110-113.
37. K. W. Schwarz, R. W. Stark, Phys. Rev. Lett., Vol. 22, No. 24, (1969), pp. 1278-1280.

38. J. A. Northby, Ph.D. thesis, University of Minnesota, 1966, (unpublished).
39. J. A. Northby, T. M. Sanders, Phys. Rev. Lett., Vol. 18, (1967), p. 1184.
40. C. L. Zipfel, Ph.D. thesis, University of Michigan, 1969, unpublished.
41. C. L. Zipfel, T. M. Sanders, in Proceedings of the 11th International Conference on Low Temperature Physics, edited by J. F. Allen, D. M. Finlayson, and D. M. McCall (St. Andrews University, St. Andrews, Scotland, (1969), p. 296.
42. C. C. Grimes, G. Adams, Phys. Rev., Vol. B41, (1990), p. 6366.
43. C. C. Grimes, G. Adams, Phys. Rev., Vol. B45, (1992), p. 2305.
44. G. Baym, R. G. Barrera, C. J. Pethick, Phys. Rev. Letters, Vol. 22, No. 1, (1969), pp. 20-23.
45. D. G. Henshaw, A. D. B. Woods, Phys. Rev. Lett., Vol. 121, (1961), p. 1266.
46. F. London, *Superfluids* (Dover Publications, New York, 1964), Vol. III.
47. G. Baym, R. G. Barrera, C. J. Pethick, Phys. Rev. Lett., Vol. 22, No. 1, (1969), pp. 20-23.
48. L. C. Shi, J. A. Kong, *Applied Electromagnetism*, Brooks/Cole Engineering Division, Monterey, CA, (1983), pp. 210-215.
49. C. S. M. Doake, P. W. F. Gribbon, Phys. Lett., Vol. 30A, No. 4, (1969), pp. 251-253.
50. G. G. Ihas, T. M. Sanders, Phys. Rev. Lett., Vol. 27, (1971), p. 383.
51. G. G. Ihas, T. M. Sanders, in Proceedings of the 13 th International Conference on Low Temperature Physics, editors K. D. Timmerhaus, W. J. O'Sullivan and E. F. Hammel, Plenum, New York, (1972), Vol. 1, p. 477.
52. G. G. Ihas, Ph.D. thesis, University of Michigan, 1971.
53. V. L. Eden, P. V. E. McClintock, Phys. Lett., Vol. 102A, No. 4, (1984), pp. 197-200
54. V. L. Eden, M. Phil. thesis, University of Lancaster, 1986.

Table 1. The calculated electric (per electron), magnetic (per electron), and ionization energies for some two-electron atoms.

Atom	r_1 (a_o)[a]	Electric Energy[b] (eV)	Magnetic Energy[c] (eV)	Calculated Ionization Energy[d] (eV)	Experimental[e] Ionization Energy (eV) [32-33]
He	0.567	-23.96	0.63	24.59	24.59
Li^{+}	0.356	-76.41	2.54	75.56	75.64
Be^{2+}	0.261	-156.08	6.42	154.48	153.89
B^{3+}	0.207	-262.94	12.96	260.35	259.37
C^{4+}	0.171	-396.98	22.83	393.18	392.08
N^{5+}	0.146	-558.20	36.74	552.95	552.06
O^{6+}	0.127	-746.59	55.35	739.67	739.32
F^{7+}	0.113	-962.17	79.37	953.35	953.89

[a] from Equation (136)
[b] from Equation (138)
[c] from Equation (139)
[d] from Equations (137) and (140)

Table 2. The first few spherical harmonics and $\frac{N_{\ell,m_\ell}}{N_{0,0}}$ of Eq. (177) as a function of ℓ, and m_ℓ.

Spherical Harmonics $Y^{\ell}_{m_\ell}$	ℓ	m_ℓ	$\frac{N_{\ell,m_\ell}}{N_{0,0}}$
$Y^0_0 = \frac{1}{(4\pi)^{1/2}}$	0	0	1
$Y^0_1 = \left(\frac{3}{4\pi}\right)^{1/2}\cos\theta$	1	0	$\sqrt{3}$
$Y^1_1 = \left(\frac{3}{8\pi}\right)^{1/2}\sin\theta e^{i\phi}$	1	1	$\sqrt{\frac{3}{2}}$
$Y^{-1}_1 = \left(\frac{3}{8\pi}\right)^{1/2}\sin\theta e^{-i\phi}$	1	- 1	$\sqrt{\frac{3}{2}}$
$Y^0_2 = \left(\frac{5}{16\pi}\right)^{1/2}\left(3\cos^2\theta - 1\right)$	2	0	$\sqrt{\frac{5}{4}}$
$Y^1_2 = \left(\frac{15}{8\pi}\right)^{1/2}\left(\sin\theta\cos\theta e^{i\phi}\right)$	2	1	$\sqrt{\frac{15}{2}}$
$Y^{-1}_2 = \left(\frac{15}{8\pi}\right)^{1/2}\left(\sin\theta\cos\theta e^{-i\phi}\right)$	2	- 1	$\sqrt{\frac{15}{2}}$
$Y^2_2 = \left(\frac{15}{32\pi}\right)^{1/2}\sin^2\theta e^{2i\phi}$	2	2	$\sqrt{\frac{15}{8}}$
$Y^{-2}_2 = \left(\frac{15}{32\pi}\right)^{1/2}\sin^2\theta e^{-2i\phi}$	2	- 2	$\sqrt{\frac{15}{8}}$

Table 3. The mobility of an excited state electron bubble having a fraction principal quantum number ($n = \frac{1}{\text{integer}}$) relative to the normal electron bubble as a function of quantum numbers n, ℓ, and m_ℓ given by Eq. (182). The peaks that appear in Figure 16 and Table 4 are indicated.

n	$\ell = 0$	$\ell = 1$ $m_\ell = 0$	$\ell = 1$ $m_\ell = \pm 1$	$\ell = 2$ $m_\ell = 0$	$\ell = 2$ $m_\ell = \pm 1$	$\ell = 2$ $m_\ell = \pm 2$
$\frac{1}{2}$	2.21 peak # 8	1.22 peak # 3	1.81 peak # 5			
$\frac{1}{3}$	3.12 peak # 10	1.92 peak # 6	2.66	2.86	1.14 peak # 2	2.41
$\frac{1}{4}$	3.81 peak # 11	2.52 peak # 9	3.33	3.54	1.60 peak # 4	3.06
$\frac{1}{5}$	4.33 peak # 12	3.03	3.86	4.07	2.03 peak # 7	3.59
$\frac{1}{6}$	4.74 peak # 13	3.47	4.28	4.49	2.41	4.02
$\frac{1}{7}$	5.07 peak # 14	3.83	4.63	4.83	2.75	4.38
$\frac{1}{8}$	5.34 peak # 15	4.15	4.93	5.12	3.06	4.68
$\frac{1}{9}$	5.57 peak # 15	4.42	5.17	5.35	3.34	4.94
$\frac{1}{10}$	5.76 peak # 15	4.66	5.38	5.56	3.59	5.16
$\frac{1}{11}$	5.92 peak # 15	4.87	5.56	5.73	3.82	5.35
$\frac{1}{12}$	6.07 peak # 15	5.05	5.72	5.88	4.02	5.52
$\frac{1}{100}$	7.75 peak # 15	7.55	7.69	7.72	7.29	7.65

Table 4. The migration times and experimental mobilities of the 15 ion peaks shown in Figure 16 relative to the normal ion with their assignments to excited state electron bubbles with quantum numbers n, ℓ, and m_ℓ and theoretical mobilities given in Table 3.

Peak #	Migration Time (Arbitrary Units)	Mobility Relative to Peak #1	Theoretical Mobility Relative to Peak #1	Assignment n, ℓ, and m_ℓ.
1	9.8	1.00	1	$n=1\ \ell=0\ m_\ell=0$
2	8.2	1.20	1.14	$n=\frac{1}{3}\ \ell=2\ m_\ell=\pm1$
3	7.6	1.29	1.22	$n=\frac{1}{2}\ \ell=1\ m_\ell=0$
4	6.2	1.58	1.6	$n=\frac{1}{4}\ \ell=2\ m_\ell=\pm1$
5	5.4	1.81	1.81	$n=\frac{1}{2}\ \ell=1\ m_\ell=\pm1$
6	5	1.96	1.92	$n=\frac{1}{3}\ \ell=1\ m_\ell=0$
7	4.85	2.02	2.03	$n=\frac{1}{5}\ \ell=2\ m_\ell=\pm1$
8	4.35	2.25	2.21	$n=\frac{1}{2}\ \ell=0\ m_\ell=0$
9	3.9	2.51	2.52	$n=\frac{1}{4}\ \ell=1\ m_\ell=0$
10	3.3	2.97	3.12	$n=\frac{1}{3}\ \ell=0\ m_\ell=0$
11	2.8	3.50	3.81	$n=\frac{1}{4}\ \ell=0\ m_\ell=0$
12	2.1	4.67	4.33	$n=\frac{1}{5}\ \ell=0\ m_\ell=0$
13	2	4.90	4.74	$n=\frac{1}{6}\ \ell=0\ m_\ell=0$
14	1.8	5.44	5.07	$n=\frac{1}{7}\ \ell=0\ m_\ell=0$
15	1.3	7.54	7.75	$n=\frac{1}{100}\ \ell=0\ m_\ell=0$

Figure Captions

Figure 1. The orbitsphere is a two dimensional spherical shell with the Bohr radius of the hydrogen atom.

Figure 2. The current pattern of the orbitsphere from the perspective of looking along the z-axis. The current and charge density are confined to two dimensions at $r_n = nr_1$. The corresponding charge density function is uniform.

Figure 3. The orbital function modulates the constant (spin) function (shown for t = 0; cross-sectional view).

Figure 4. Far field approximation.

Figure 5. The magnetic field of an electron orbitsphere.

Figure 6. Broadening of the spectral line due to the rise-time and shifting of the spectral line due to the radiative reaction. The resonant line shape has width Γ. The level shift is $\Delta\omega$.

Figure 7. The Cartesian coordinate system wherein the first great circle magnetic field line lies in the yz-plane, and the second great circle electric field line lies in the xz-plane is designated the photon orbitsphere reference frame of a photon orbitsphere.

Figure 8. The field line pattern from the perspective of looking along the z-axis of a right-handed circularly polarized photon.

Figure 9. The electric field of a moving point charge ($v = \frac{4}{5}c$).

Figure 10. The electric field lines of a right-handed circularly polarized photon orbitsphere as seen along the axis of propagation in the lab inertial reference frame as it passes a fixed point.

Figure 11. The front view of the magnitude of the mass (charge) density function in the xy-plane of a free electron; side view of a free electron along the axis of propagation--z-axis.

Figure 12. The experimental results for the elastic differential cross section for the elastic scattering of electrons by helium atoms and a Born approximation prediction.

Figure 13. The closed form function (Eqs. (145) and (146)) for the elastic differential cross section for the elastic scattering of electrons by helium atoms. The scattering amplitude function, $F(s)$ (Eq. (144), is shown as an insert.

Figure 14. The mobility from the data of Ihas [2, 52] of electron bubbles in superfluid helium plotted versus the inverse of the temperature. Solid triangles are for the normal electron bubble, open squares, circles, triangles and solid circles are for the four ions of the same peak assigned in Figure 16 and Table 4.

Figure 15. The mobility (Eq. (182)) of an excited state electron bubble having a fraction principal quantum number $(n = \frac{1}{\text{integer}} = 1/p)$ relative to the normal electron bubble as a function of p for given ℓ, and m_ℓ quantum numbers.

Figure 16. Data trace from Ihas [52] showing the detected ion signal as a function of time. N and F denote the normal and fast ion peaks. The peaks labeled 1 to 15 are assigned in Table 4. For a description of experimental condition see Ihas [52].

Figure 17. Data traces from Eden and McClintock [53] of the current at the collector of the velocity spectrometer (arbitrary units) as a function of the elapsed time t after a pulse was applied to release exotic ions. Signals are shown for a range of strong electric fields as indicated in units of $10^5\ V/m$ by the number above each trace. The steep rise on the right-hand sides of the signals indicates the arrival of the normal ion current. For a description of experimental condition see Eden and McClintock [53].

Figure 18. The limiting electron bubble velocities shown in the data traces of Figure 17 relative to the normal electron bubble as a function of p corresponding to principal quantum number $n = \frac{1}{\text{integer}} = 1/p$ where $\ell = 0$, and $m_\ell = 0$.

Fig. 1

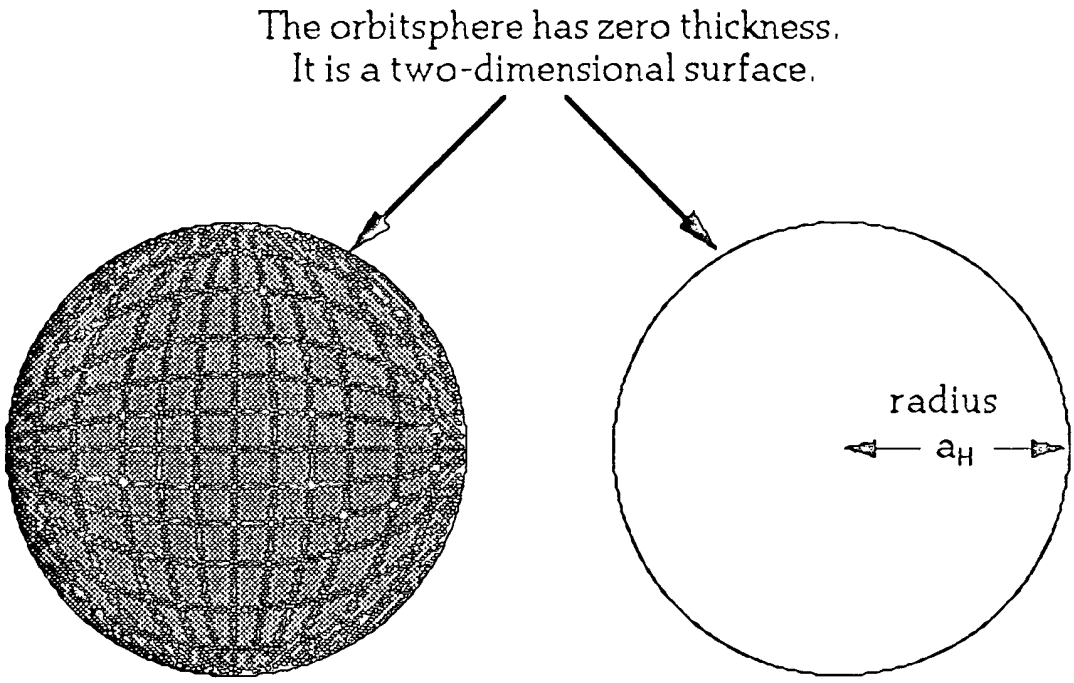
The orbitsphere has zero thickness.
It is a two-dimensional surface.
radius
a_H

Fig. 2

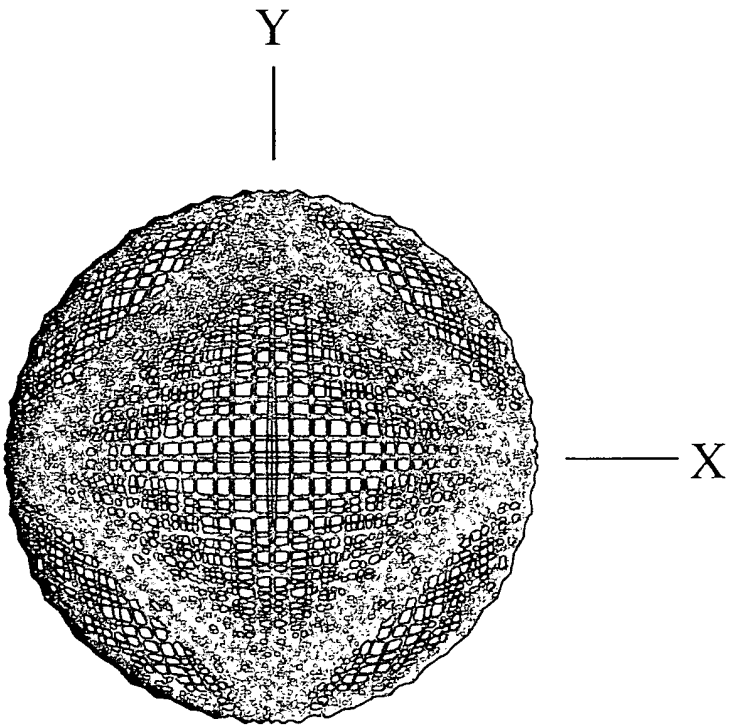

VIEW ALONG THE Z AXIS

Fig. 3

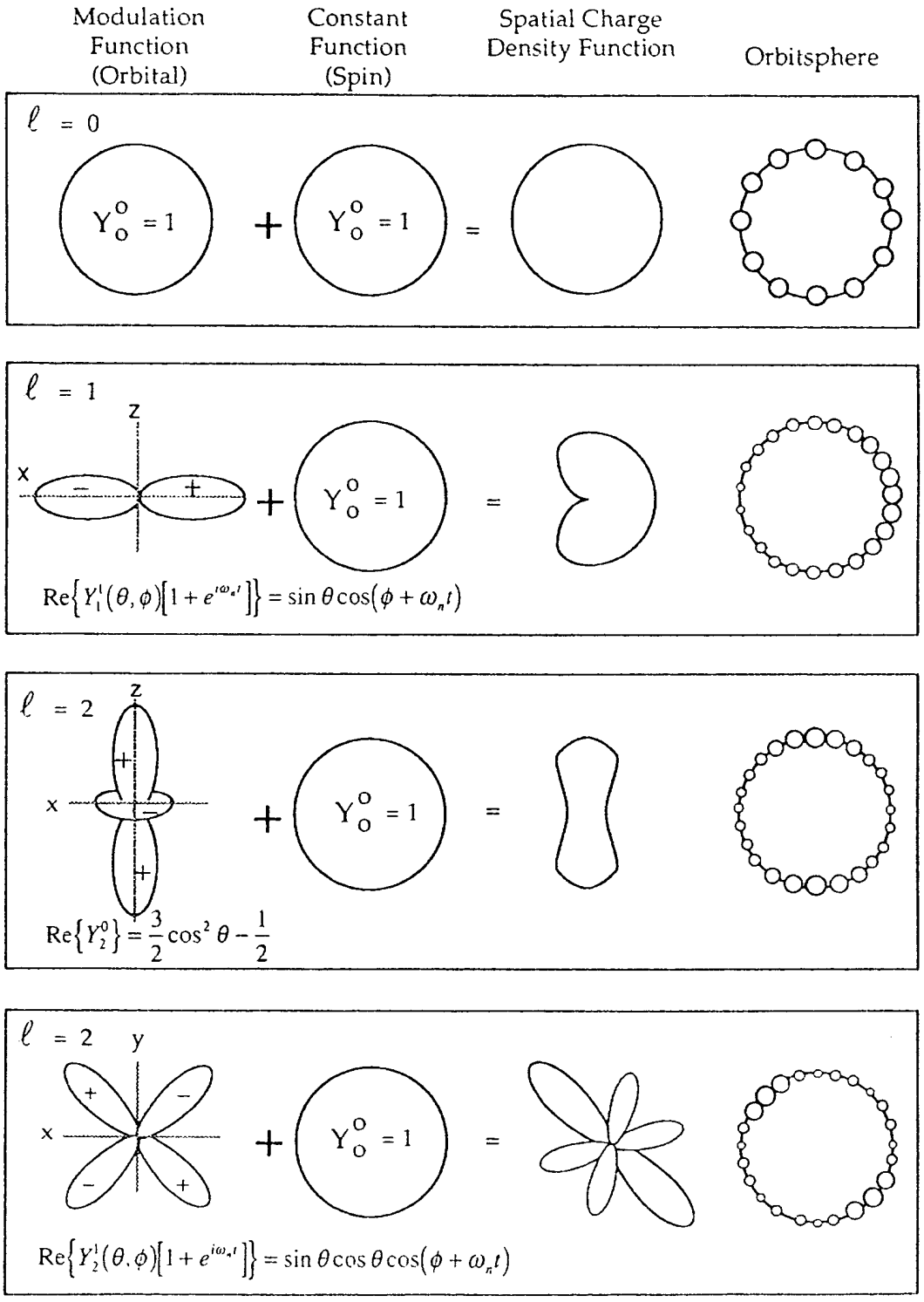
Modulation Function (Orbital)
Constant Function (Spin)
Spatial Charge Density Function
Orbitsphere
ℓ = 0
$Y_o^o = 1$
+
$Y_o^o = 1$
=
ℓ = 1
z
x
−
+
$Y_o^o = 1$
=
$\mathrm{Re}\left\{Y_1^1(\theta,\phi)\left[1+e^{i\omega_n t}\right]\right\} = \sin\theta\cos(\phi+\omega_n t)$
ℓ = 2
z
x
+
−
+
$Y_o^o = 1$
=
$\mathrm{Re}\left\{Y_2^0\right\} = \frac{3}{2}\cos^2\theta - \frac{1}{2}$
ℓ = 2
y
x
+
−
−
+
$Y_o^o = 1$
=
$\mathrm{Re}\left\{Y_2^1(\theta,\phi)\left[1+e^{i\omega_n t}\right]\right\} = \sin\theta\cos\theta\cos(\phi+\omega_n t)$

Fig. 4

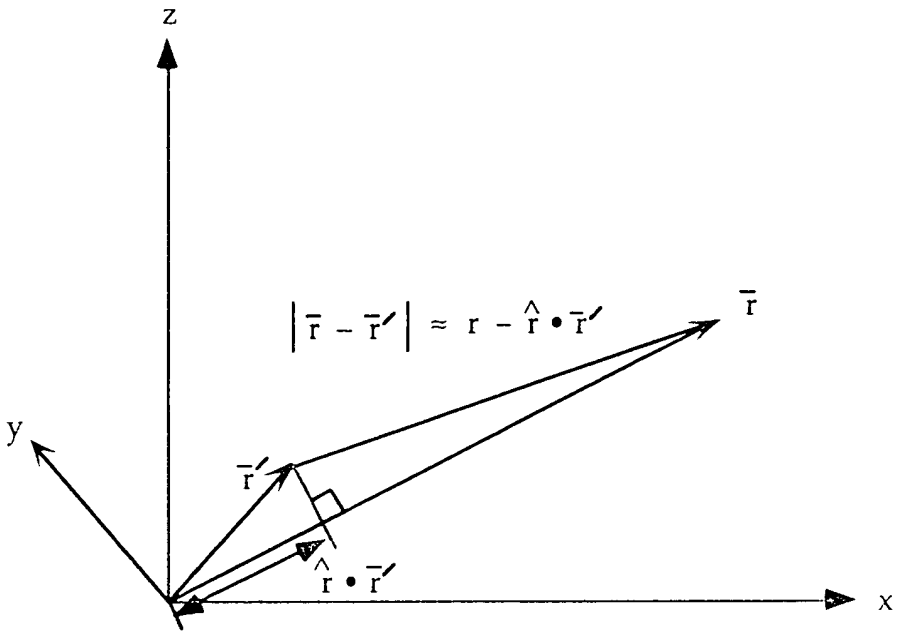
z
y
x
$\bar{r}$
$\bar{r}'$
$\hat{r} \cdot \bar{r}'$
$|\bar{r} - \bar{r}'| \approx r - \hat{r} \cdot \bar{r}'$

Fig. 5

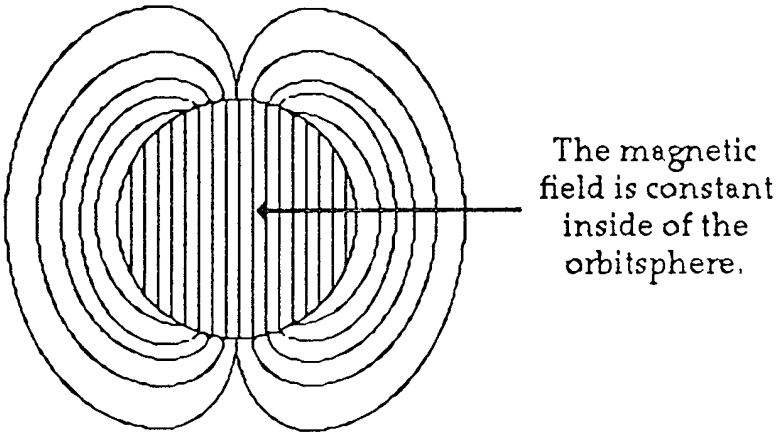

Fig. 6

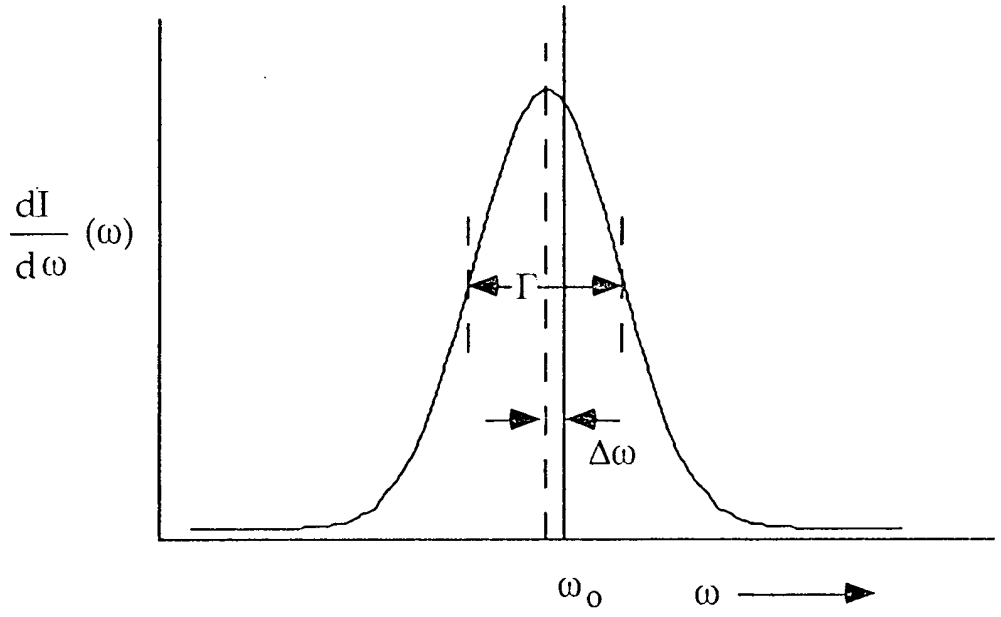

Fig. 7

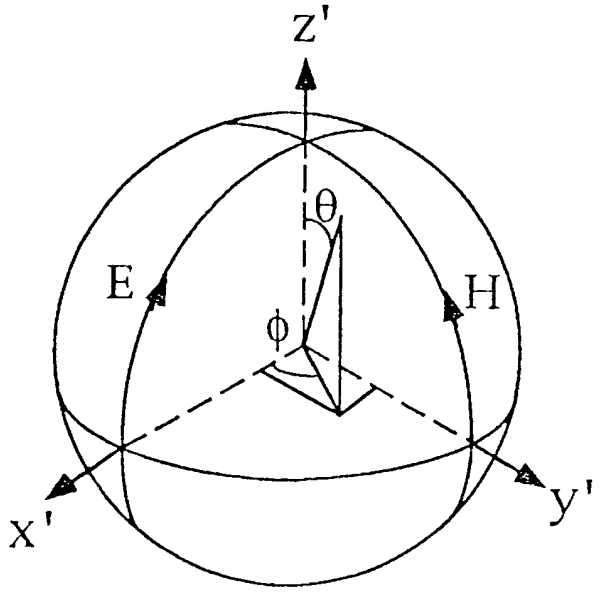

Fig. 8

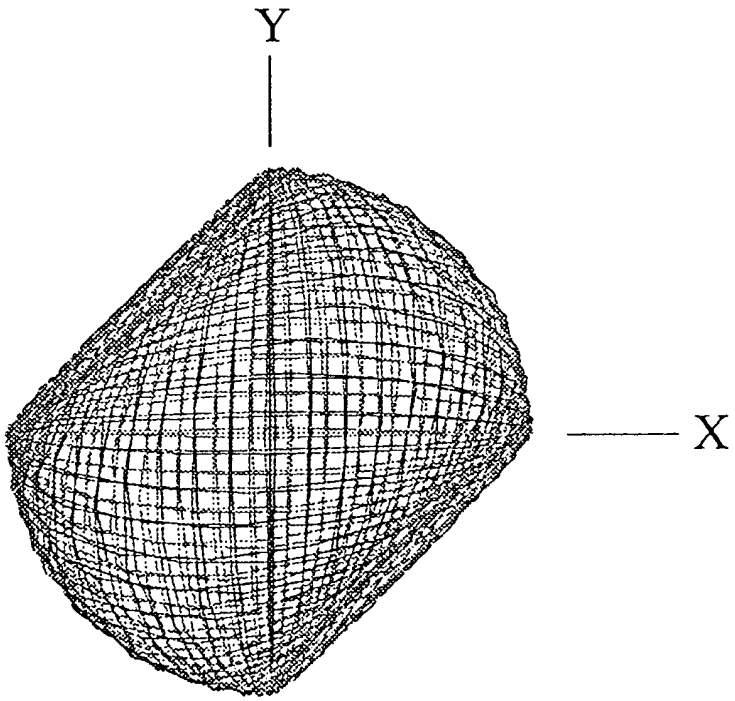

VIEW ALONG THE Z AXIS

Fig. 9

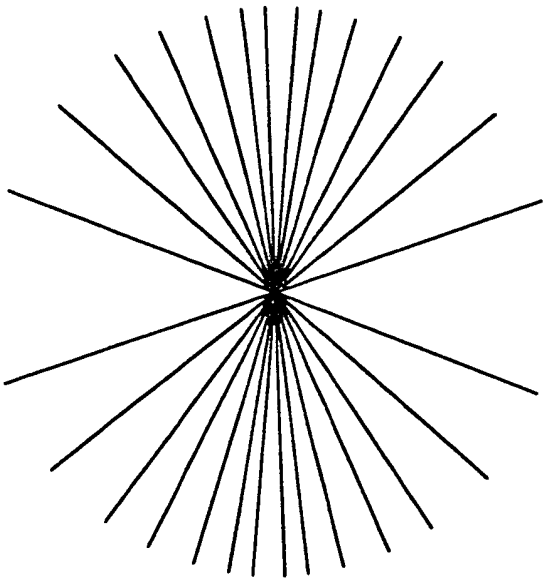

Fig. 10

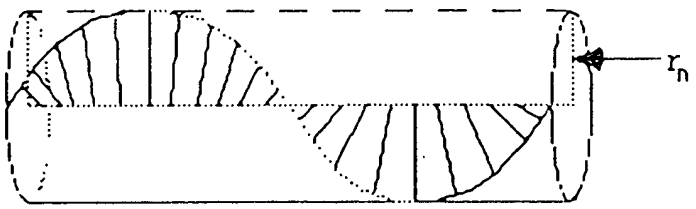

$$2 \pi r_n = \lambda_n$$

Fig. 11

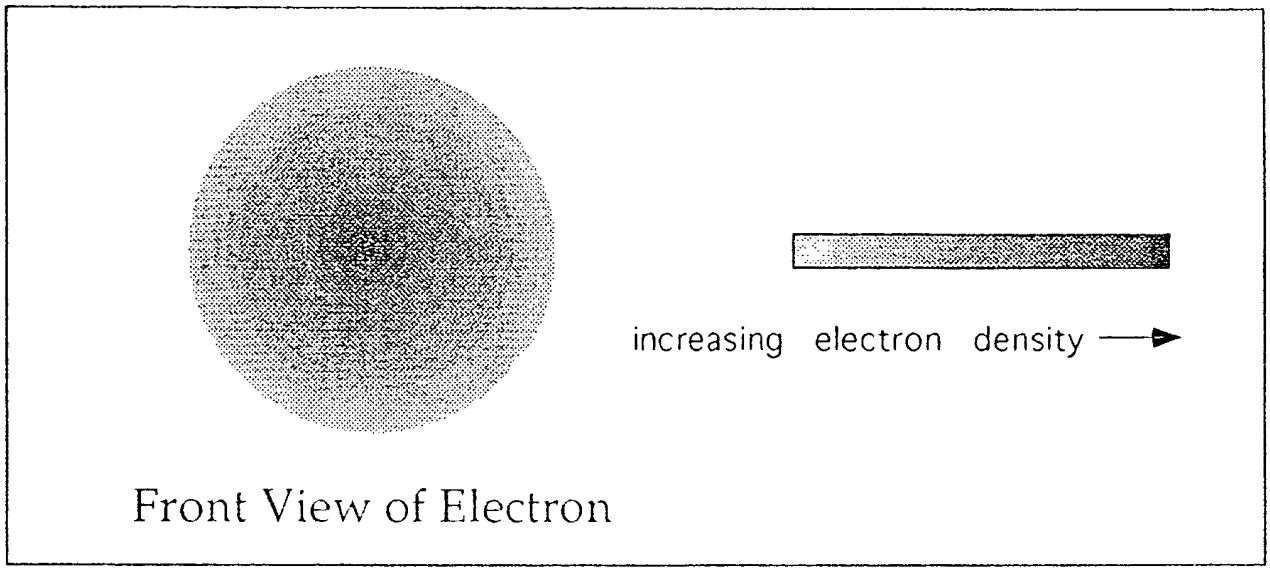

$$\rho_0 = \frac{\hbar}{mv_z}$$

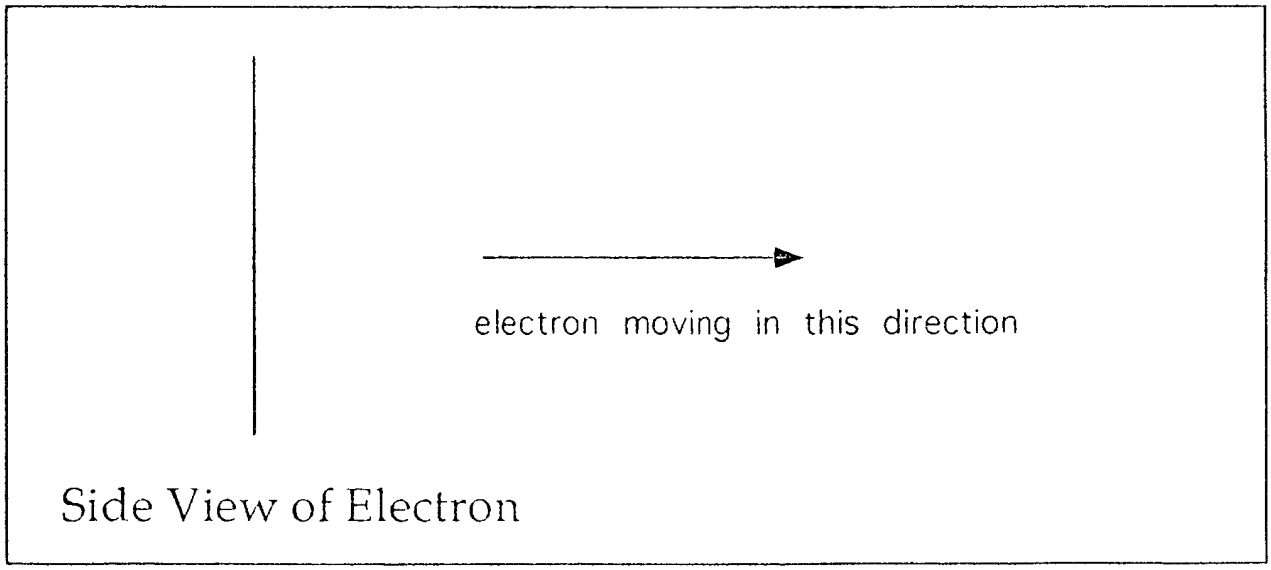

Fig. 12

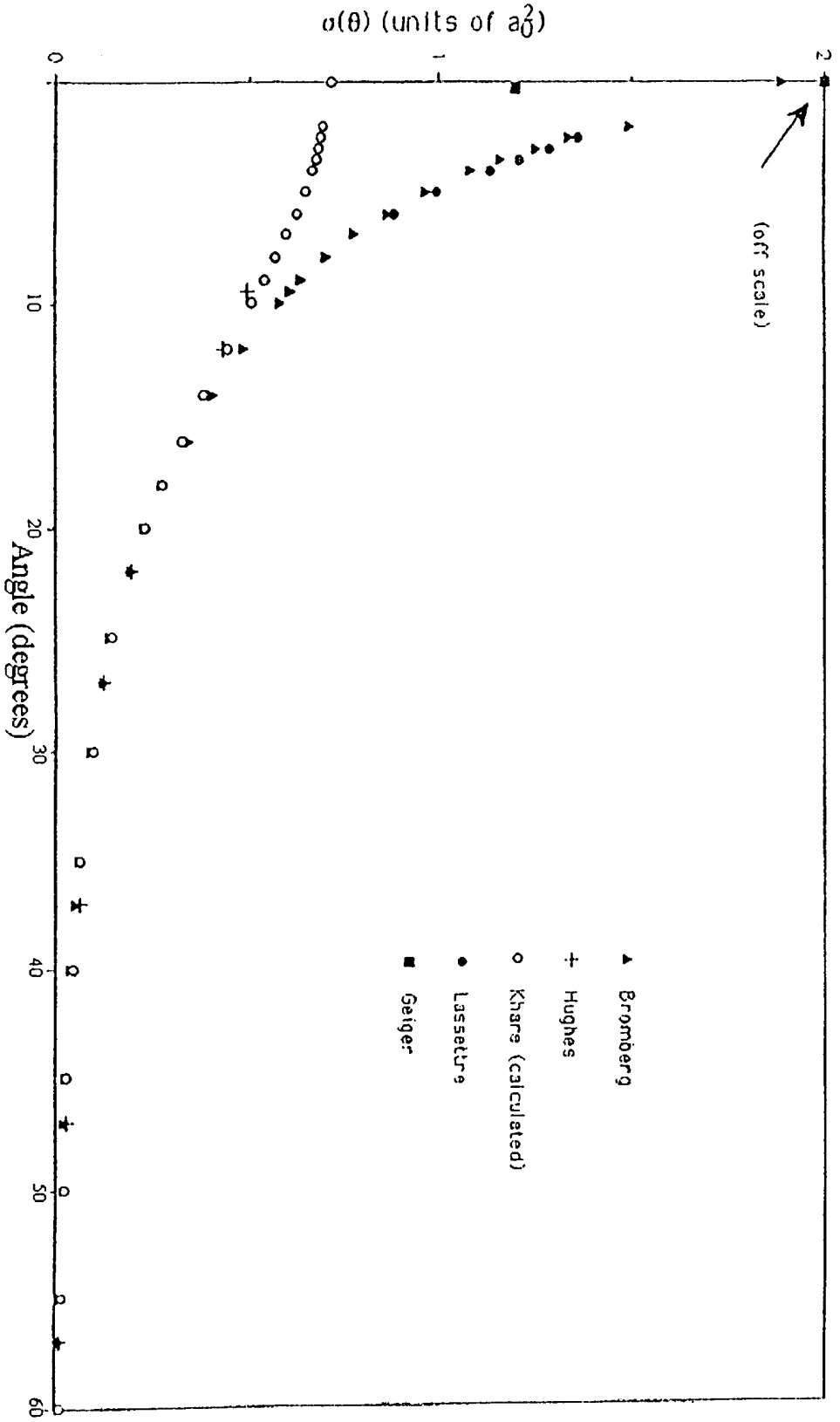
σ(θ) (units of a_0^2)
0
1
2
(off scale)
10
20
30
40
50
60
Angle (degrees)
Bromberg
Hughes
Khare (calculated)
Lassettre
Geiger

Fig. 13

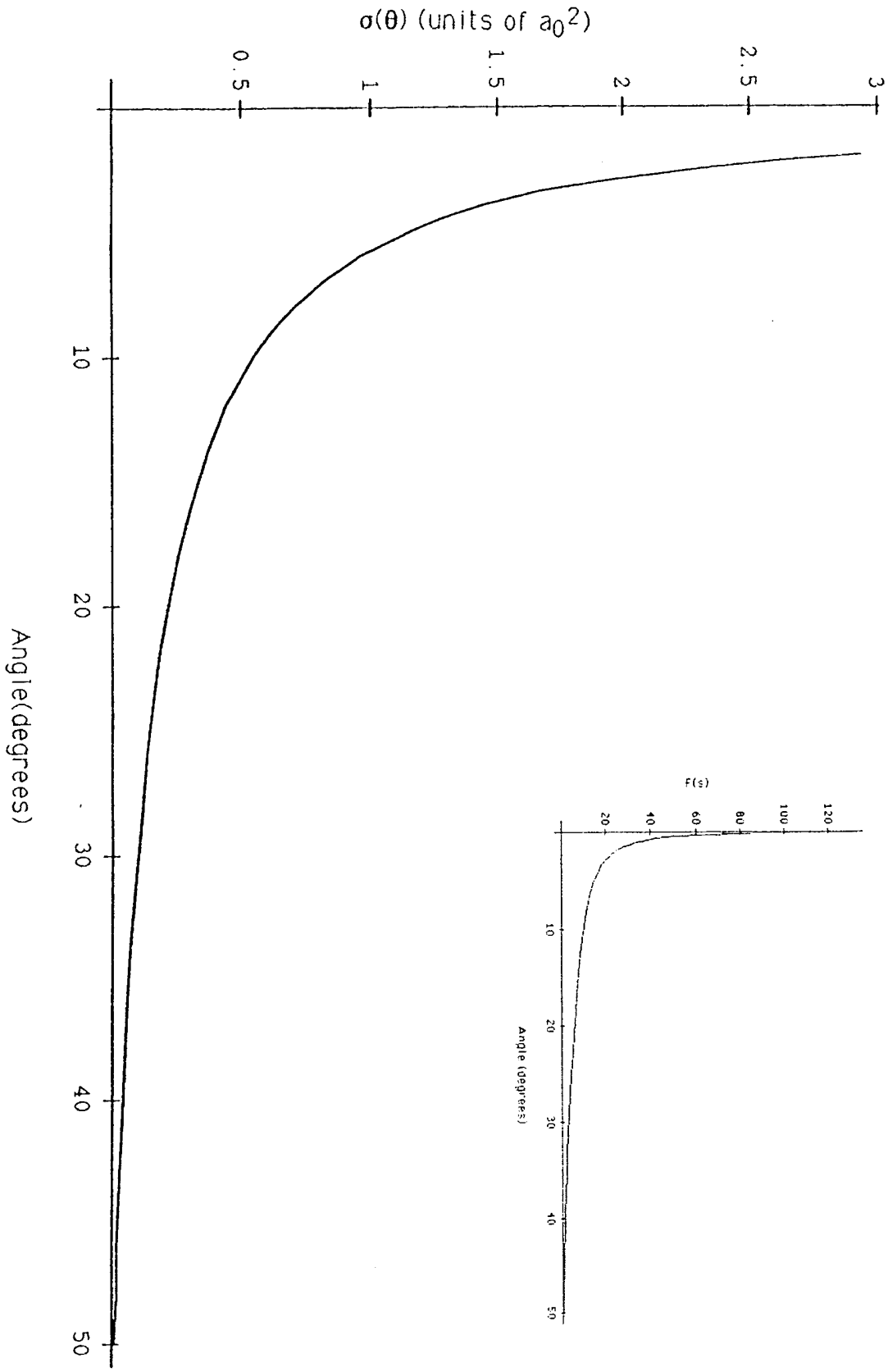
σ(θ) (units of a_0^2)
0.5
1
1.5
2
2.5
3
10
20
30
40
50
Angle(degrees)
F(s)
20
40
60
80
100
120
10
20
30
40
50
Angle (degrees)

Fig. 14

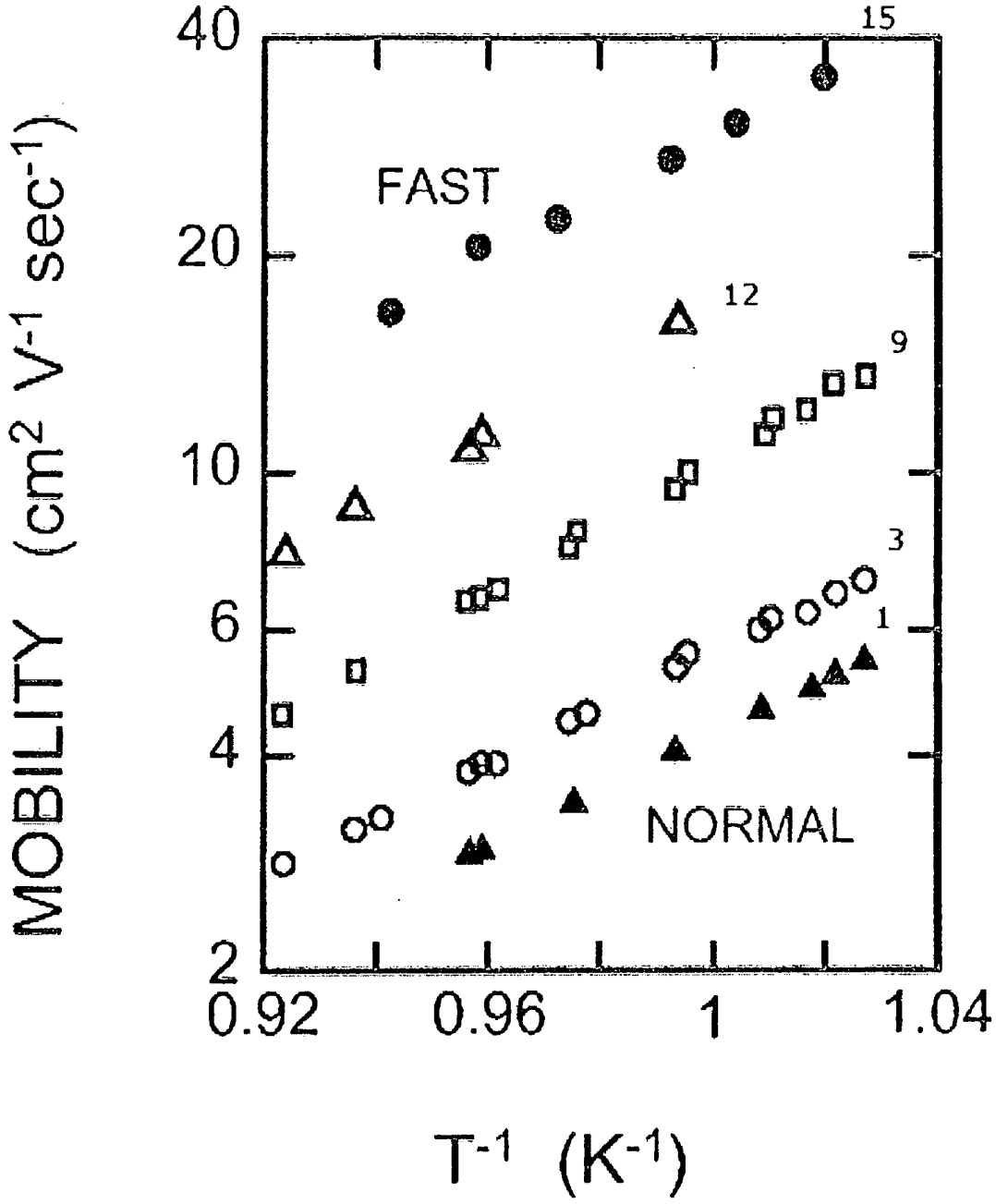
MOBILITY (cm² V⁻¹ sec⁻¹)
40
20
10
6
4
2
FAST
NORMAL
15
12
9
3
1
0.92
0.96
1
1.04
T⁻¹ (K⁻¹)

Fig. 15

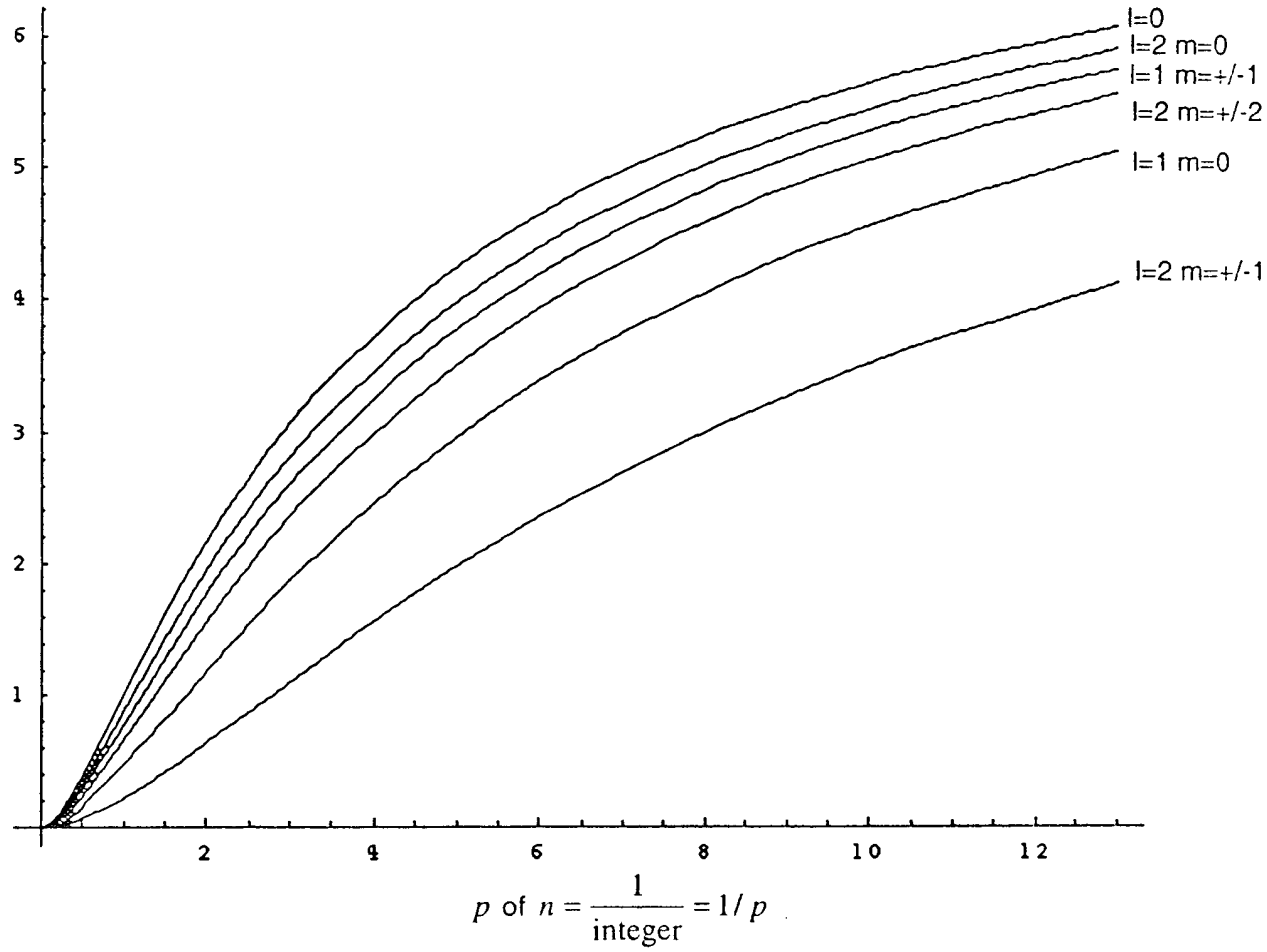
l=0
l=2 m=0
l=1 m=+/-1
l=2 m=+/-2
l=1 m=0
l=2 m=+/-1
6
5
4
3
2
1
2
4
6
8
10
12
p of n = 1/integer = 1/p

Fig. 16

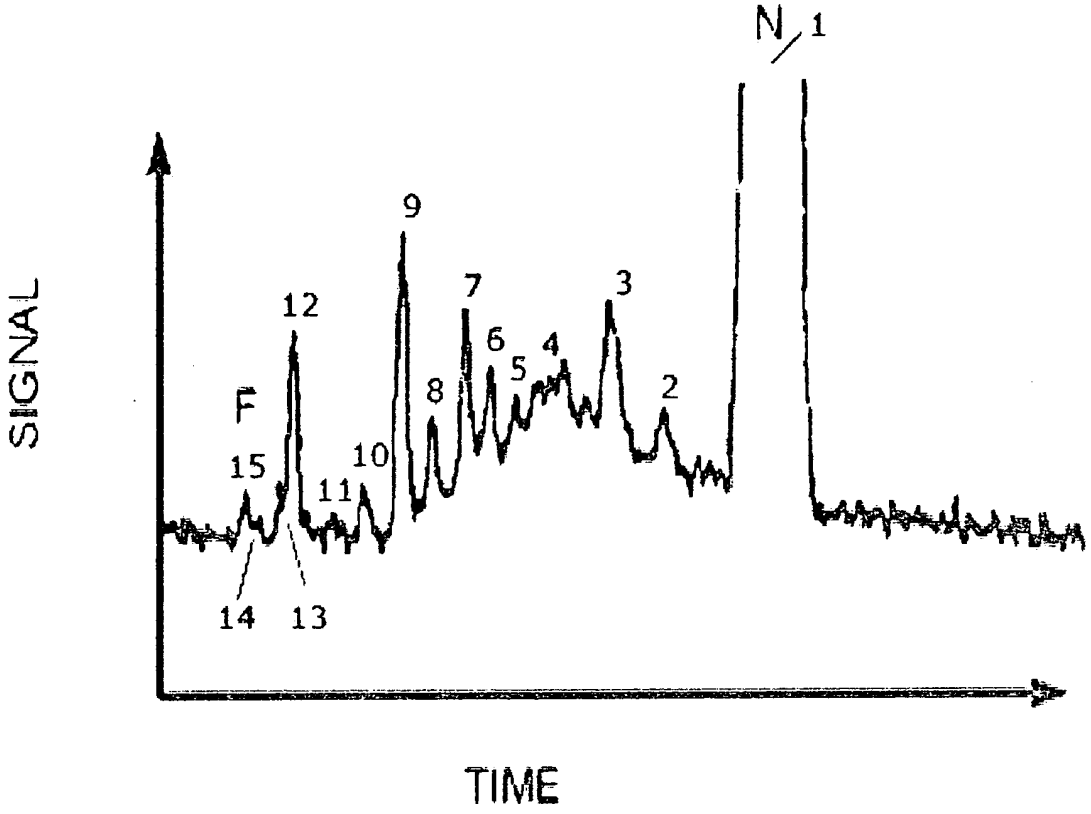

Fig. 17

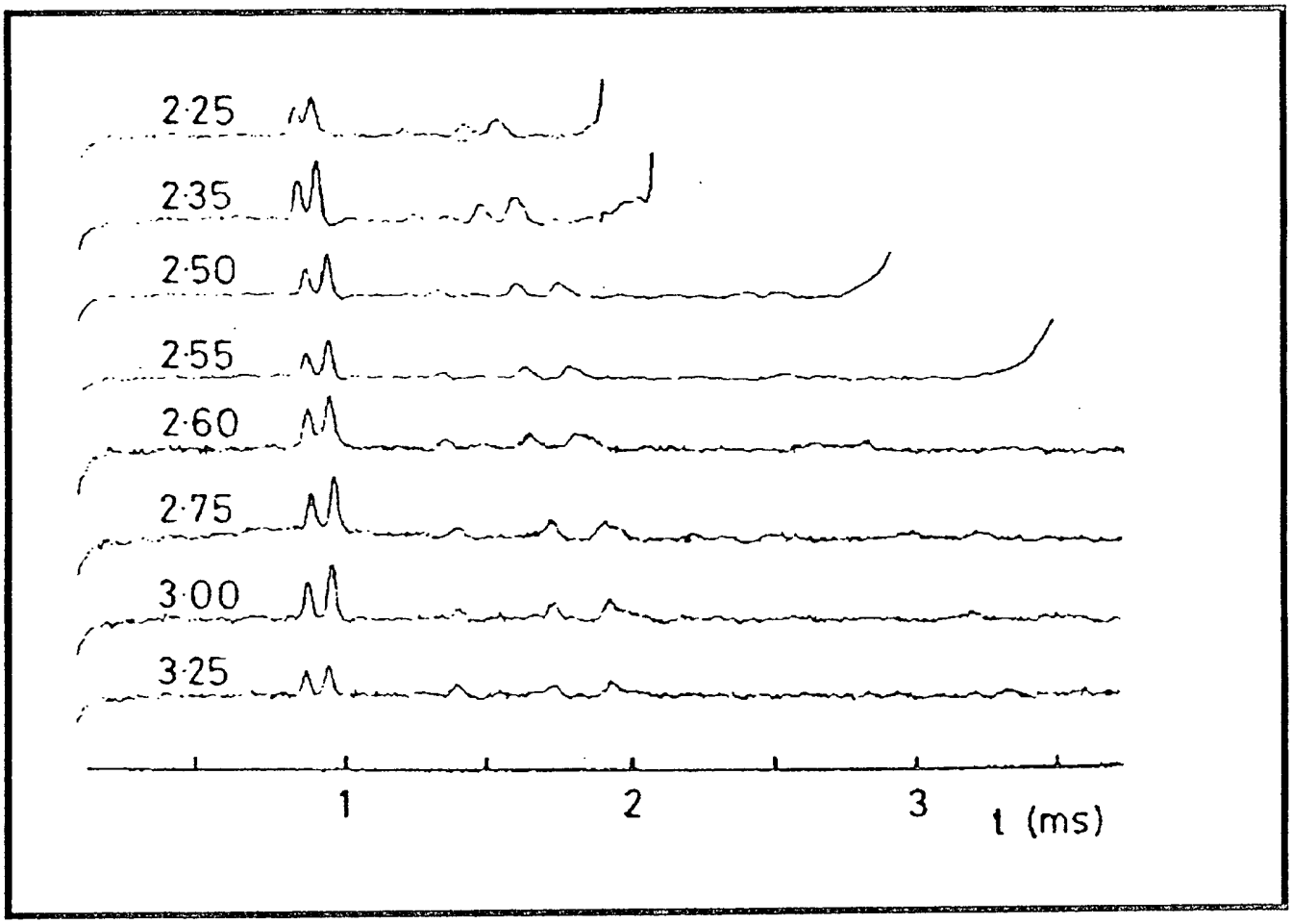

Fig. 18

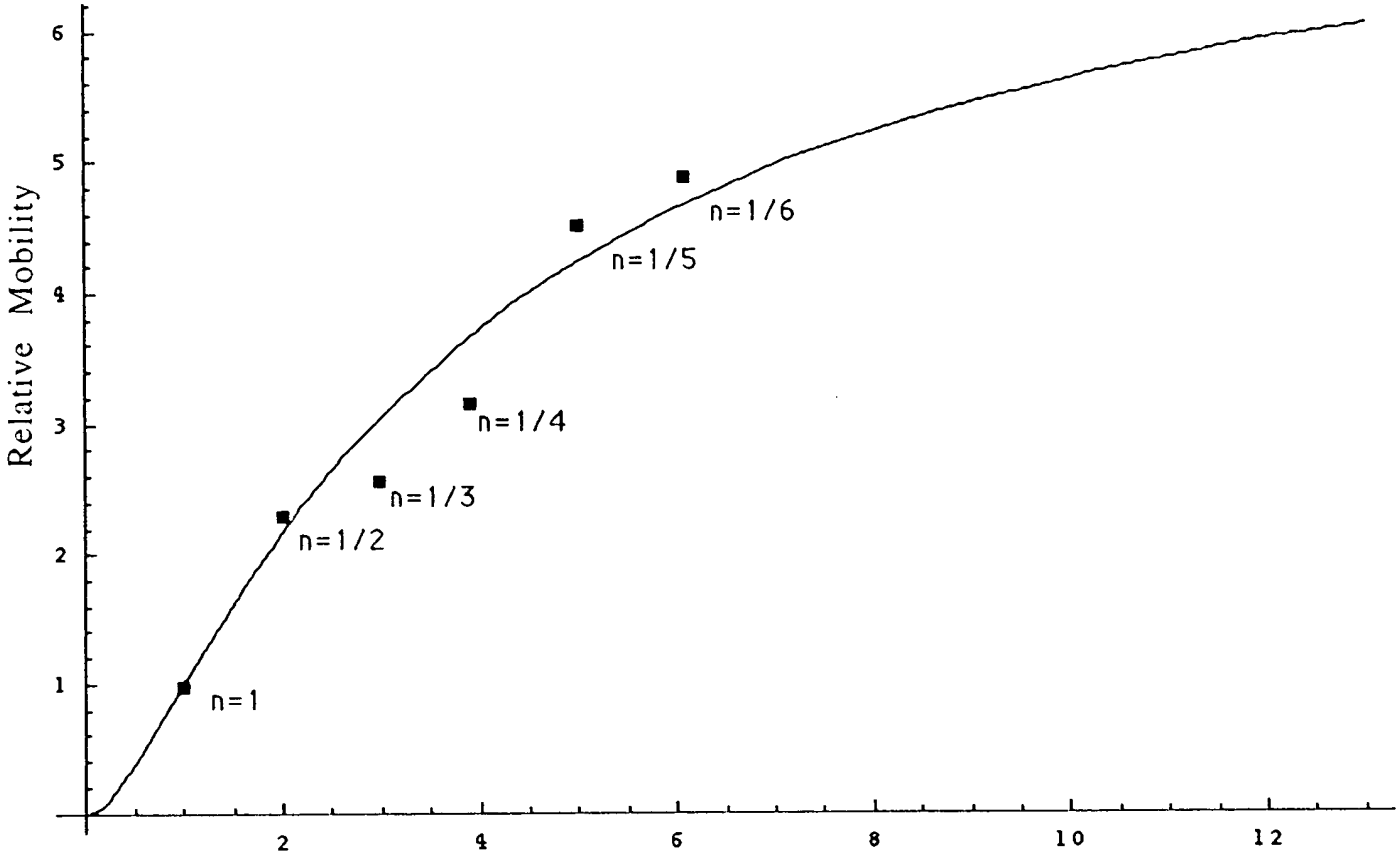

$$p \text{ of } n = \frac{1}{\text{integer}} = 1/p$$